Journal of Materials Processing Tech. 332 (2024) 118563

Contents lists available at ScienceDirect

Journal of Materials Processing Tech.

journal homepage: www.elsevier.com/locate/jmatprotec

Reduction of sawing forces in bone cutting: Innovative oscillating saw mechanism based on trajectory analysis

Han Wang, Urara Satake *, Toshiyuki Enomoto

Division of Mechanical Engineering, Graduate School of Engineering, Osaka University, 2-1, Yamada-oka, Suita, Osaka 565-0871, Japan

ARTICLE INFO

Keywords:
Bone sawing
Impact force
Ploughing force
Oscillating sawing
Trajectory design

ABSTRACT

Oscillating bone sawing is a critical procedure in orthopedic surgery. However, conventional oscillating saw mechanisms often result in excessive sawing forces, which are detrimental to implant fixation and postoperative patient recovery. Therefore, there is an urgent need to design a new oscillating saw mechanism to reduce sawing forces during surgery, including avoiding ineffective impact forces on bone cutting and preventing ploughing forces caused by negative rake angle contact with the workpiece. In this study, an innovative oscillating sawing mechanism is proposed to effectively inhibit the generation and accumulation of impact forces, avoid negative rake angle contact with the workpiece. Oscillating sawing experiments under various cutting conditions demonstrated that the proposed mechanism significantly reduces cutting forces and prevents defects due to crack propagation of the bone and saw teeth damage. The proposed design offers an effective mechanism to achieve small and stable sawing forces in bone sawing surgery, and it inspires tailored oscillating saw techniques for specific machining needs, such as thin deep groove cutting.

1. Introduction

Oscillating sawing is an essential bone cutting technique in orthopedic surgeries such as fracture repair, joint replacement, and orthognathic surgery [1]. Its reciprocating motion allows for precise cutting of hard tissues, e.g., cortical bone and cancellous bone, within confined surgical spaces and minimizes the risk of damage to surrounding soft tissues [2]. However, excessive bone cutting forces can influence postoperative recovery and surgical outcomes. For instance, in total knee arthroplasty (TKA), the most prevalent joint replacement, surgeons typically begin by drilling to place a positioning pin within the knee joint and then use a cutting guide block to precisely position the saw blade for creating a flat implant surface at the correct orientation for implant bonding. However, the low rigidity of the saw blade (e.g., 1 mm thickness and 110 mm length) results in significant cutting forces, making it difficult to securely control an oscillating saw and leading to blade deflection [3]. This deflection can cause uneven implant surfaces, potentially leading to implant component misalignment [4], reduced longevity, and patient discomfort. Consequently, surgeons often need to perform corrective rework to achieve proper alignment, thereby increasing surgical time [5]. Alternatively, using bone cement to fill uneven surfaces may result in loosened implant components. Increasing blade thickness enhances rigidity, as seen in robotic-arm-assisted surgeries, but this also elevates cutting forces or reduces feed rates, thereby prolonging operation time. Moreover, excessive cutting forces can cause the saw blade being kicked out from the bone, posing risks to surrounding soft tissues [5,6]. Furthermore, these forces may fracture bones due to their semi-brittle nature [7,8], induce thermal [9,10] and mechanical damage [11], and cause bone debris buildup on tools due to localized heat generation [12,13]. Complications may also arise from blade wear [12,14], affecting cutting precision and potentially causing inaccuracies, exacerbated by surgeon fatigue [5,15] or insufficient rigidity in robotic-arm systems. Therefore, reducing cutting forces in oscillating sawing is crucial.

Cortical bone, the tough outer layer of bone, significantly influences cutting forces and is commonly used in bone cutting studies. Its characteristics such as semi-brittle behavior, anisotropy due to osteon orientation, and low thermal conductivity have been extensively studied in relation to cutting forces [16]. Different osteon orientations can affect the direction of cracks propagation. By controlling the direction of crack propagation, it is possible to achieve lower specific cutting forces [17]. Additionally, crack propagation at different cutting depths also

* Corresponding author.
E-mail addresses: wanghan@cape.mech.eng.osaka-u.ac.jp (H. Wang), satake@mech.eng.osaka-u.ac.jp (U. Satake), enomoto@mech.eng.osaka-u.ac.jp (T. Enomoto).

https://doi.org/10.1016/j.jmatprotec.2024.118563
Received 5 July 2024; Received in revised form 9 August 2024; Accepted 16 August 2024
Available online 22 August 2024

influences chip formation and increasing the cutting depth can also reduce specific cutting forces [18]. A larger positive rake angle will significantly reduce cutting forces and cutting heat [19]. Based on these studies, tools aimed at reducing overall cutting forces have been proposed for bone milling [20,21] and drilling [22].

However, due to the significant differences between oscillating sawing and rotary cutting methods, reducing overall cutting forces using large cutting depths is challenging. Milling cutters generally machine the flat surface of the bone by side milling [23], which means that the cutter can use a large depth of cut to complete the rough milling before using a small depth of cut to avoid damage to the machined surface. In contrast, oscillating sawing directly cuts through bone to provide a machined surface suitable for mounting an implant (e.g., the artificial knee), necessitating the prevention of surface cracking during the cutting process. On the other hand, oscillating sawing introduces the ploughing force due to the negative rake angle of the flank face [24,25] or rounded cutting edge [26,27] on the saw teeth, which can become excessive with a large cutting depth. During reciprocating motion, as a large positive rake angle is used, the negative rake angle on flank face also increases, thereby significantly increasing the ploughing force, which greatly hinders the reduction of total cutting forces.

The sawing force is influenced by the interaction between the teeth during oscillation, which is determined by the alignment of the tooth tips and the oscillating trajectory [24,28,29]. Initially, the curved edge saw blade was widely used due to the evenly distributed force on each tooth tip as the same oscillating radius. However, serious problems: clogging due to bad chip evacuation [12,24], blade are easily kicked out from the bone (resulting in a "kicking" phenomenon) due to the curved edge easily generate one side force [30]. To address this issue, Fletcher and Fisher [30] patented a saw blade with a straight blade edge (US6503253B1) to reduce the “kicking” phenomenon. It was found that this design also improved chip evacuation to avoid clogging [24]. Subsequently, a saw blade with a concave edge shape was developed to further address the kicking problems [5]. However, these straight or concave edge shapes, due to the differing oscillating radius of each tooth tip, generated different cutting depths for each tooth tip, resulting in a larger sawing force compared to blades with curved edge shapes [24]. By analyzing the trajectory of the saw tooth tips, Wang et al. [29] further identified that the increased force is primarily due to significant impact near the extremes of oscillation between the saw teeth and the workpiece. Additionally, the sawing force model proposed by Wang et al. [29] considers three components of the sawing force: the cutting force generated by effectively cutting the workpiece, the ploughing force resulting from the elastic deformation of the workpiece due to negative rake angle, and the impact force generated by compressing the workpiece. This model reveals that a significant portion of the applied force may not contribute to chip formation but rather translates into elastic deformation and crack propagation, thereby increasing the overall sawing force. Particularly during stopped groove cutting, the impact force increases linearly with the feed. When stopped groove cutting is performed on only one side, resulting in an unbalanced sawing force in the oscillation direction, the saw blade may encounter resistance from the impact, causing the bone to be kicked out and risking injury to the surrounding soft tissue [5,6]. When stopped groove cutting is performed on both sides, the impact force increases on both the left and right sides. This can lead to brittle bone parts breaking or even sharp bone debris flying out quickly, posing serious risks to the patient’s recovery and increasing the potential for bioaerosol contaminants and infection for the surgeon [31].

Previous studies have demonstrated that reducing cutting forces and increasing cutting efficiency is possible by improving the oscillating trajectory. James et al. [2] designed a figure-eight orbital motion to provide a larger depth of cut per tooth for improving cutting efficiency. However, a larger depth of cut poses a higher risk of causing crack propagation due to the large impact force. Additionally, they mentioned that the additional stroke in the thrust direction carries a risk of rebounding from the bone surface, leading to erratic cutting conditions. Carusillo [32] hold a patent (US9572585B2) with a similar trajectory to facilitate chip evacuation. Shu et al. [33] proposed the elliptical vibration-assisted motion into conventional oscillating sawing which shows a great reduction of cutting force. However, the higher vibration frequency may induce increased friction, leading to higher temperature rise [7] and potentially causing burns in bone tissue when a high thrust force is applied [34]. Overall, these innovative methods, while effective in reducing cutting forces or increasing cutting efficiency, did not specifically address the challenges posed by ploughing force and impact force, which can lead to excessive cutting forces. This limitation restricted the extent to which cutting forces could be reduced. Therefore, optimizing the trajectory of saw teeth to minimize impact force and ploughing force remains crucial.

In this study, an innovative oscillating saw mechanism was proposed based on a comprehensive analysis of tooth tip trajectories to reduce sawing forces, particularly impact force and ploughing force that did not contribute to chip formation. A method was introduced to incorporate a reverse feed motion near the extremes of oscillation, altering the cutting depth and rake angle of the tooth tip to break off continuous chips from the workpiece, thereby avoiding the accumulation of impact force. Additionally, saw blade tooth tip positions aligned according to the proposed motion trajectory to avoid contact between the negative rake face of the tooth tips and the workpiece, reducing ploughing force. The bone cutting comparison experiment with conventional oscillating sawing mechanisms demonstrated the excellent performance of the newly designed oscillating sawing mechanism, showing significant reductions in impact and ploughing forces, thus avoidance of cracks on the machined surface on workpieces and saw teeth damages. The proposed mechanism will significantly advance current oscillating sawing techniques in bone cutting surgery and inspire tailored oscillating saw techniques for specific machining needs, such as thin deep thin groove cutting.

2. Improvement for oscillating sawing mechanism

2.1. Conventional oscillating sawing mechanism

Fig. 1 shows the conventional oscillating sawing process. The oscillating unit drives a saw blade with multiple saw teeth at the end, which oscillates repeatedly around a pivot point and feeds forward to cut the workpiece (Fig. 1a). Depending on the width of the workpiece and the oscillating range of the blade, either a through groove or a stopped groove is formed [29]. In both situations, the ploughing force cannot be ignored. When the tooth tip oscillates in the opposite direction, the actual rake face of the tooth tip changes to a large negative rake angle, resulting in the generation of a ploughing force (Fig. 1b).

In the case of a stopped groove, the corners on both sides form a compressed zone (Fig. 1a) because the workpiece is compressed by the outermost teeth of the saw blade without being entirely removed, resulting in the generation of a significant impact force. Although Winter [35] patented (US3905374A) a redesigned saw blade with outermost teeth having a positive rake angle oriented outward to reduce the impact force, significant impact forces still occurred in a single-tooth sawing experiment [29]. The conventional trajectory of a single tooth tip (Fig. 1b) shows that the instantaneous depth of cut of tooth tip gradually increases from one extreme of the oscillation to the other side thus generate a continuous chip when using a positive rake face [25]. When the tooth tip moves to the extreme of the oscillation, the root of the chip is not separated from the bone but compressed and accumulated to the corner, thus the cutting force is converted into impact force, which is absorbed by the elastic deformation of the bone. In addition, the impact force is related to the contact area of the tooth tip with the workpiece and the distance at which elastic deformation occurs, which both increased as feed, thus resulting in an increasing impact force [29].

Previous research has shown that impact forces increase linearly

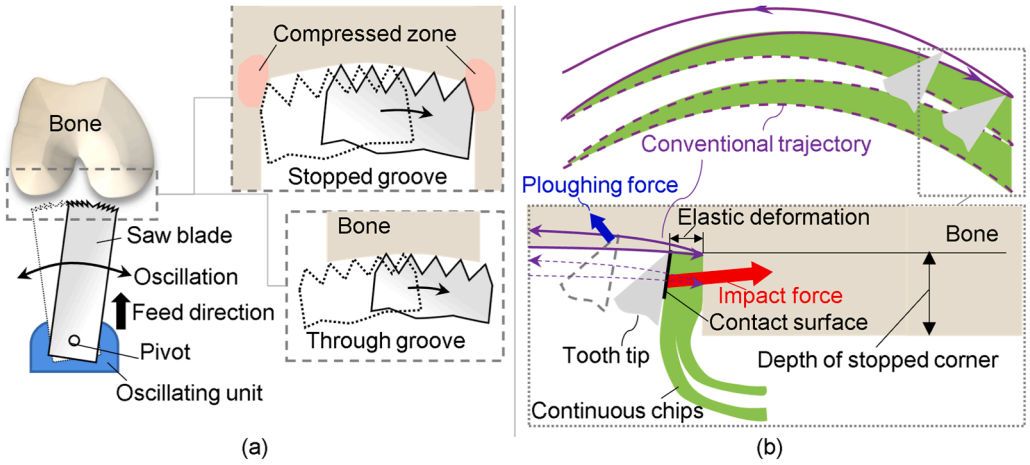

Fig. 1. Schematic diagram of the conventional oscillating sawing mechanism. (a) Stopped and through grooving in the conventional oscillating sawing process. (b) Conventional trajectory causing impact force and ploughing force.

with the stopped corner depth, even when using a zero-rake angle (Fig. 2a, adapted from [29]). At a stopped corner depth of only 200 μm, the impact force on a single tooth reaches 30 N. If the impact force continues to increase linearly, it would reach 160 N at 1 mm (Fig. 2a). Given that cortical bone thickness is generally greater than 1 mm and feed rates are usually over 1 mm/s, it may be challenging for the surgeon to withstand such a significant impact force over a short period. This could lead to undesirable outcomes, as discussed in Section 1.

On the other hand, the cutting force on each saw tooth is influenced by adjacent teeth, which alters the instantaneous depth of cut due to overlapping trajectories [28,29]. The instantaneous depths of cut of two typical saw blade edge shapes—curved-edge and straight-edge—are shown in Fig. 3a, b.

The machined area of the outermost tooth when cutting outwards (A_P) is not affected by the trajectory of the adjacent teeth, generating a large impact force for both curved-edge and straight-edge saw blades. When oscillating from the outside to the inside, the machined area of the outermost tooth (A_N) produces a significant difference: the curved-edge saw blade results in a smaller depth of cut due to the adjacent tooth having the same oscillation radius, thus producing a smaller ploughing force compared to the straight-edge saw blade. In contrast, the straight-edge saw blade creates a larger depth of cut with a negative rake angle, leading to greater ploughing and impact forces.

For the teeth other than the outermost ones, the curved-edge saw

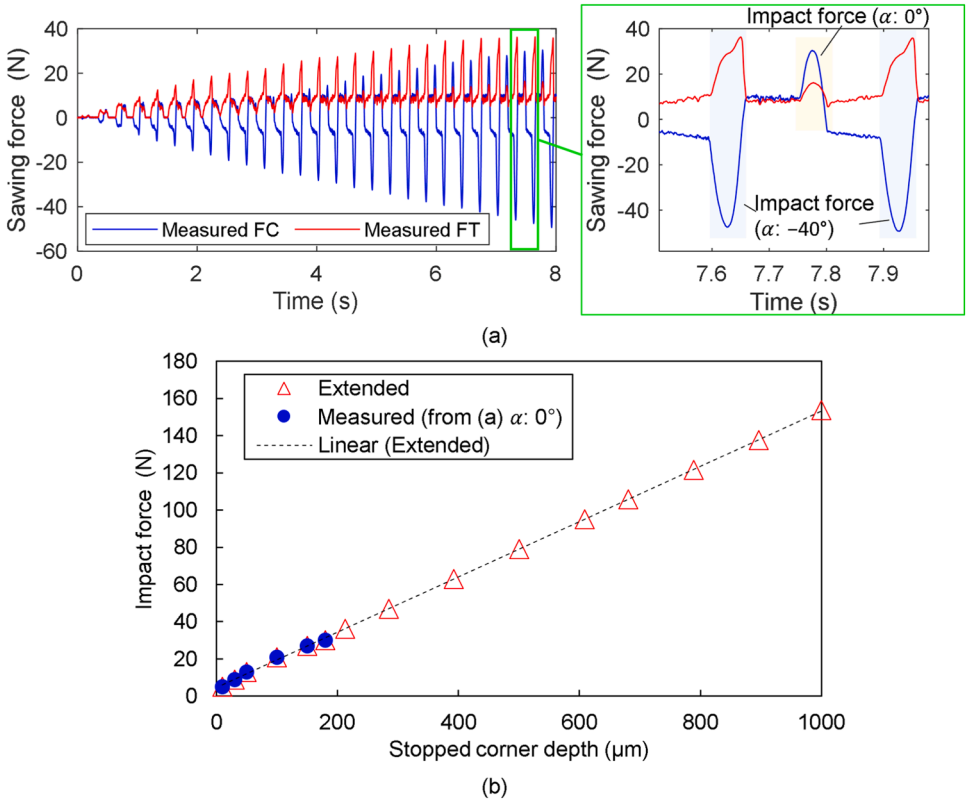

Fig. 2. Impact force increases linearly with the stopped corner depth. (a) Oscillating sawing forces in a stopped groove cutting on cortical bone with a single-tooth blade [29]. Parameters: depth per oscillating cycle: 10 μm; tooth rake angles: 0° and −40°; FC: principal force in oscillation direction, FT: thrust force in feed direction. (b) Linear trend of the measured impact force (zero-rake angle, FC) with increasing stopped corner depth.

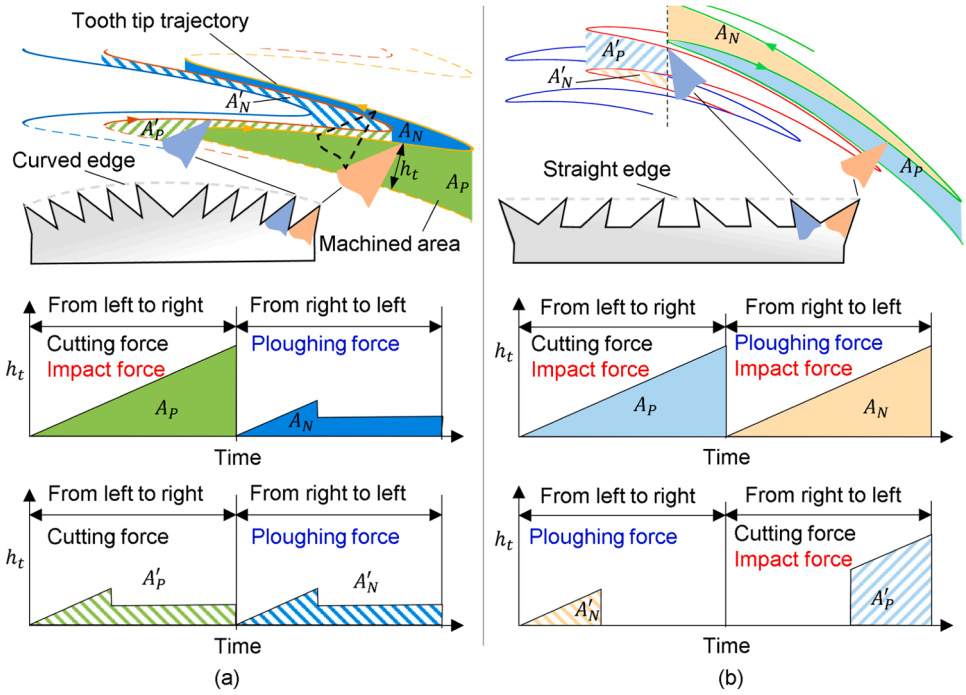

Fig. 3. Machined area and depth of cut of a single tooth tip with different edge saw blades. (a) Curved-edge blade (b) Straight-edge blade [29]. A_P, A_N are the machined area of the outermost tooth with positive and negative rake angles, respectively; A'_P, A'_N are the machined area of the rest teeth with positive and negative rake angles, respectively; h_t is the instantaneous depth of cut of the tooth tip.

blade produces a continuous and relatively small depth of cut across the machined areasA'_P and A'_N (Fig. 3a), meaning each tooth generates relatively small cutting and ploughing forces. Conversely, the straight-edge saw blade generates practical machined areas A'_P and A'_N (Fig. 3b) only near the extremes of the oscillation inward, as the middle portion of the machined area has already been removed by adjacent tooth tips with larger oscillation radii. Therefore, the tooth tips on the left and right sides are alternate and discontinuous in generating the cutting force and ploughing force. In addition, due to the different oscillation radii, the tooth tips also generate an impact force in machined area A'_P, thus causing an impact force on each tooth.

In summary, these two typical saw blades generate impact force and ploughing force to varying degrees that do not contribute to chip removal. In particular, the impact force can increase with the depth of the stopped corner. Effectively leveraging the differences in cutting depth variation between these two blade edge shapes can help mitigate the generating impact force and ploughing force, resulting in smaller and stable sawing forces.

2.2. New oscillating mechanism concept for reducing sawing force

Based on the analysis in Section 2.1, it can be considered that avoiding the impact force and ploughing force near extremes of the oscillation can effectively reduce the overall sawing force. As shown in Fig. 4a, to avoid the impact force, the instantaneous of cutting depth in machined area A'_P should be decreased to facilitate the chip separate from workpiece in each oscillating cycle. On the other hand, the instantaneous of cutting depth in machined area A'_N should be decreased to reduce ploughing force generated by the negative rake.

Here, as shown in Fig. 4b, a novel oscillating trajectory concept was proposed to reduce the forces near the extremes of oscillation: When the tooth moves near the extreme, a backward motion along the feed direction is added to change the cutting direction, thus further reducing the cutting depth to facilitate chip separation from the workpiece. When the tooth moves out from the extreme, instead of returning to the same path, the trajectory continues to move backward for some time before moving forward to return to the previous oscillating trajectory. This strategy can avoid negative rake angle surface contact with the workpiece and thus reduce the ploughing force.

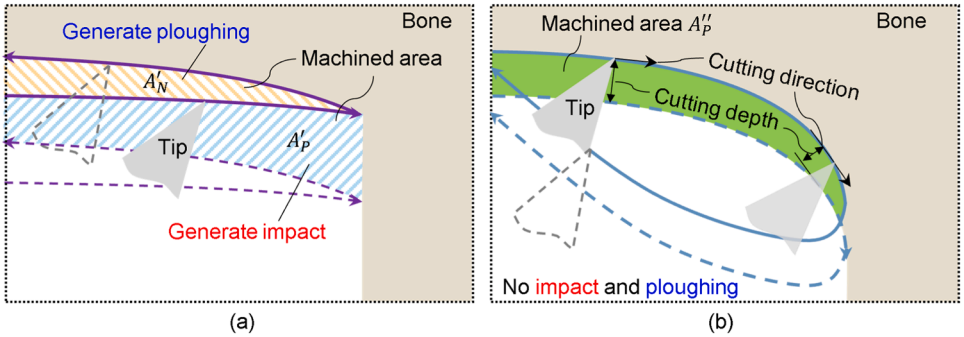

Fig. 4. Illustration of tooth trajectory and machined area near the extreme of oscillation for different mechanism concepts. (a) Conventional mechanism. (b) Proposed mechanism.

Overall, this mechanism concept modifies the trajectory near the oscillation extremes to follow an elliptical-like path, effectively reducing the sawing forces and improving the efficiency of the cutting process.

2.3. Design for new trajectory and related to saw teeth arrangement

To verify the theoretical validity of this mechanism concept, a corresponding trajectory design was proposed, and then the related saw teeth arrangement was designed considering the interaction of individual teeth.

2.3.1. New trajectory

A new proposed trajectory based on the concept mentioned in Section 2.2 as shown in Fig. 5a. The differences between it and the conventional trajectory are shown in Fig. 5b,c.

The conventional oscillating trajectory equation in the *YZ* plane of the mechanism can be expressed from [29]:

$$P_{Con}(t) = \begin{cases} Y(t) = R\sin\theta_t \\ Z(t) = R\cos\theta_t + V_{feed}t \end{cases} \quad (1)$$

$$\theta_t = C_1\sin(2\pi f_1 t) \quad (2)$$

where θ_t is the instantaneous oscillating angle with time t; C_1 is the is the amplitude angle of oscillation; f_1 is the oscillating frequency; V_{feed} is the feed speed in Z-direction; R is the oscillating radius, i.e., length between pivot and saw tooth tip. Therefore, by changing the instantaneous oscillating radius near the extremes, the elliptical-like path can be achieved, and the proposed trajectory equation ($P_{New}(t)$) can be expressed as

$$P_{New}(t) = \begin{cases} Y(t) = (R - \Delta l_t)\sin\theta_t \\ Z(t) = (R - \Delta l_t)\cos\theta_t + V_{feed}t \end{cases} \quad (3)$$

where Δl_t is the instantaneous of backward distance. Assume that the feed speed is zero and the trajectory point moves to point a (or d) near the extreme of oscillation when Δl_t begins to vary with time as a positive portion of a sinusoidal curve (Fig. 5b). As the trajectory point moves to e' when it oscillated to the extreme end, Δl_t continues to increase until it reaches point e, the lowest point of the trajectory, and then Δl_t begins to decrease until it reaches 0 at point f. Thus, Δl_t can be represented by the segmented function

$$\Delta l_t = \begin{cases} C_2\sin(2\pi f_2(t - t_d)) & , t_d < t < t_f \\ 0 & , t \le t_d \text{ or } t \ge t_f \end{cases} \quad (4)$$

where C_2 is the maximum backward distance; f_2 is the frequency for the variation of Δl_t, which can be simplified to the half value of f_1; t_d is the start time of backward motion; t_f is the time when moved to point f.

The instantaneous cutting depth of the proposed trajectory (h'_t, Fig. 5e) is different with that of the conventional trajectory (h_t, Fig. 5d). In conventional trajectory, cutting depth increases as oscillation from

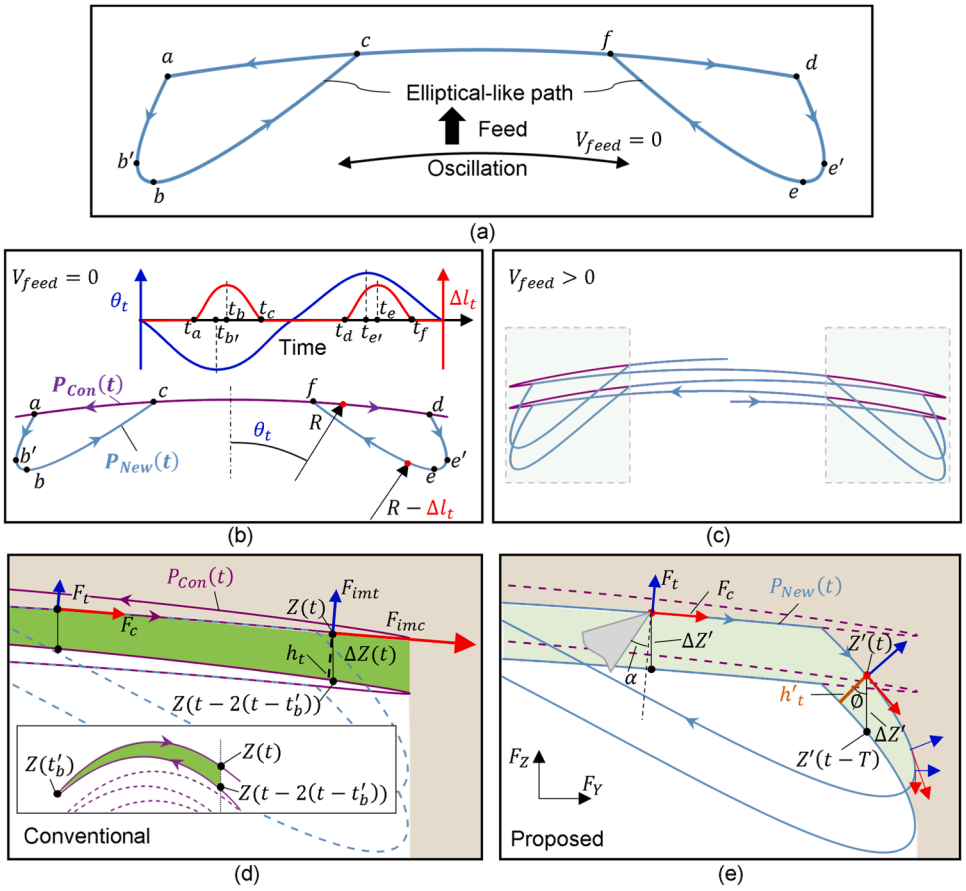

Fig. 5. Illustration of the conventional and proposed trajectories. (a) Proposed trajectory design with elliptical-like paths near the extremes of oscillation. (b-c) Comparison between conventional ($P_{Con}(t)$) and new proposed ($P_{New}(t)$) trajectories with or without feed speed. (d-e) Machined area and force variation for different trajectories on the right oscillation side of the conventional and proposed trajectories. R: oscillating radius; Δl_t: instantaneous backward distance; F_c and F_t: cutting forces along the cutting and thrust directions, respectively; F_{imc} and F_{imt}: impact force along the cutting and thrust directions, respectively; α: rake angle of the tooth; ΔZ and $\Delta Z'$: Z-axis difference of the trajectory at adjacent oscillation cycles for conventional and proposed trajectories, respectively ($\Delta Z = Z(t) - Z(t - 2(t - t'_b))$ [29], $\Delta Z' = Z(t) - Z'(t - T)$); h_t, h'_t: instantaneous cutting depth of the conventional and proposed trajectories, respectively; $\varnothing$: angle between cutting depth and Z-axis; F_Y and F_Z: sawing force in Y-axis and Z-axis, respectively.

zero to a maximum value ($h_{poc} = V_{feed}/f_1$), which can be expressed from [29]

$$h_t = Z(t) - Z\left(t - 2\left(t - t_b^{'}\right)\right) = V_{feed}(t - t_{b'})\cos\varnothing_t \tag{5}$$

where $t_{b'}$ is the time at move to left extreme of the oscillation; $\varnothing_t$: angle between cutting depth and Z-axis, which can be calculated as $\varnothing_t = \arctan\frac{dZ(t)}{dY(t)}$. While h'_t can be expressed as

$$h'_t = h_{poc}\cos\varnothing_t = h_{poc}\cos\left(\arctan\frac{dZ(t)}{dY(t)}\right) \tag{6}$$

Here, although the difference variation of cutting depths in the conventional and new proposed trajectories, the theoretical machined area for each oscillating cycle is not changed since the same feed and same oscillating range. In other words, the newly proposed mechanism does not reduce the theoretical cutting efficiency of the conventional mechanism.

Due to the actual rake angle would change to negative rake angle during backward path, the cutting forces in proposed trajectory (F_{New}) can be expressed as [36]

$$F_{New} = \begin{cases} F_{c_{new}} = \sigma_n(\mu\tan(\alpha - \varnothing_t) + 1)wh'_t \\ F_{t_{new}} = \sigma_n(\mu - \tan(\alpha - \varnothing_t))wh'_t \end{cases} \tag{7}$$

where w is the width of cutting edge; σ_n: normal stress; μ: friction coefficient; $(\alpha - \varnothing_t)$: represent the actual rake angle.

Subsequently, the sawing forces along feed direction and oscillating direction can be calculated from

$$\begin{cases} F_Y = F_t\cos|\varnothing_t| - F_c\sin|\varnothing_t| \\ F_Z = F_t\sin|\varnothing_t| + F_c\cos|\varnothing_t| \end{cases} \tag{8}$$

where F_c and F_t: cutting forces along cutting direction and thrust direction, respectively.

To clarify the variation rules of cutting direction and depth generated by the new trajectory, a series of parameter values commonly used in surgery were substituted into the trajectory equation, e.g., oscillating radius (R): 110 mm, which generally used in large bone cutting [33]; oscillating angle (C_1): ±2.55° [2]; cutting depth per oscillating cycle: 10 μm [26,37] due to feed speed (V_{feed}) at 2 mm/s [33] and oscillating frequency (f_1) at 200 Hz [26,37]. In addition, the maximum backward distance (C_2) was set as 0.35 mm, which corresponds to the value used in the experiments. Therefore, the tangent direction (cutting direction) near the right extreme can be expressed as shown in Fig. 6a. The start time of backward motion (t_d) were set as 0.6, 0.7 and 0.8 of half oscillation cycle to avoid the impact force near the extreme. The tangent direction, tangent angle and cutting depths were calculated based on Eqs. (3)–(6). As t_d decreases, the trajectory starts backward motion further away from the extreme position, i.e., avoid impact, but the tangent direction changes more slowly (Fig. 6b), which caused the depth of cut decreases less efficiently (Fig. 6c). Nonetheless, there is no doubt that it has the opposite trend to the depth of cut of conventional trajectory. Based on Eq.(8), and parameters in previous research [29] (σ_n: 1150 MPa; μ: 0.4; w: 0.8 mm), the sawing force variation near the extreme ($t_d \rightarrow t_{e'}$) of the proposed trajectory with different tool rake angles (10°, 20°, and 30°) calculated as shown in Fig. 7.

The sawing force in the oscillating direction initially increased gradually due to the actual rake angle decreasing to a negative rake

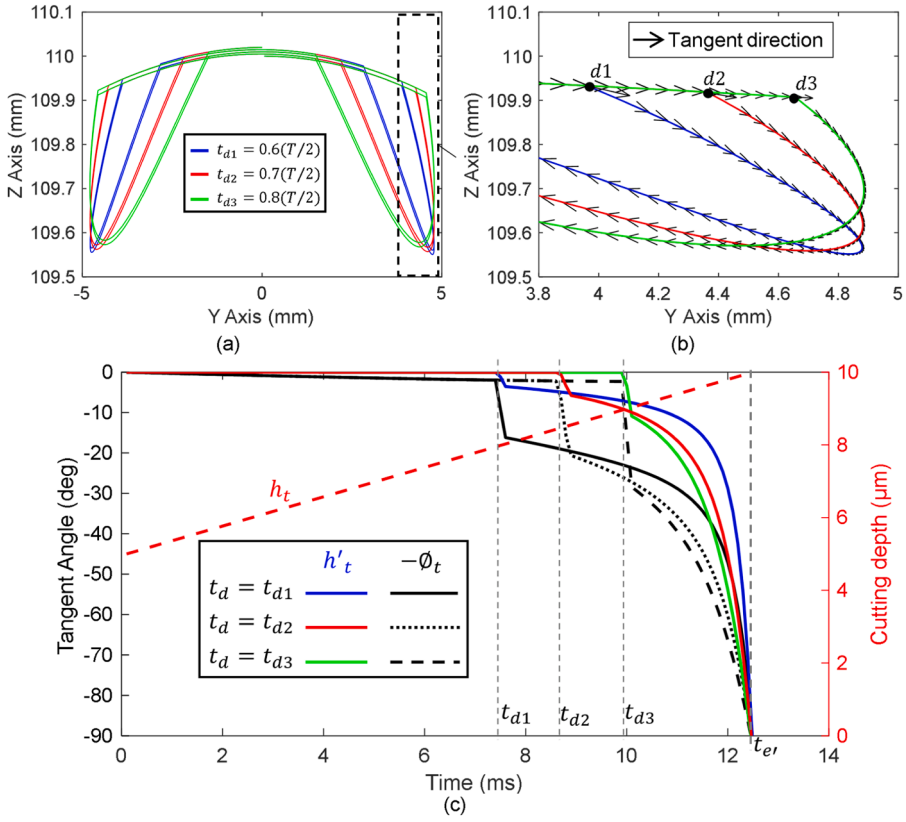

Fig. 6. Proposed trajectory and tangent angle ($-\varnothing_t$). (a) Proposed trajectory with different t_d. (b) Tangent direction of the trajectories near the extreme of oscillation. (c) Variation of tangent angle ($-\varnothing_t$), cutting depth of the proposed trajectories (h'_t) with time when setting t_d as different times, and its comparison with the cutting depth of the conventional trajectory (h_t). The trajectory starts at point (0, 110) on the YZ plane, moving from center to right side. As t_d decreases, the trajectory starts backward motion further away from the extreme position, but the tangent angle decreases more slowly, resulting in a less efficient reduction in cutting depth.

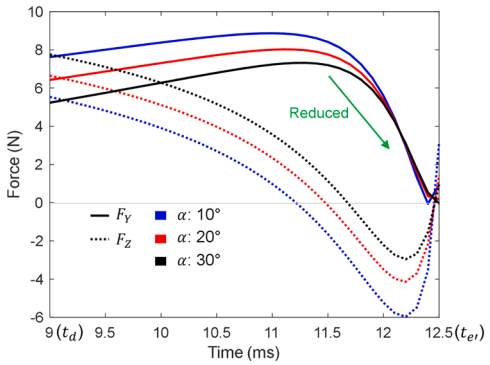

Fig. 7. Variation in calculated sawing force near the extreme ($t_d \rightarrow t_{e'}$) of the proposed trajectory for different ideal rake angles.

angle. As it neared the extreme, the cutting depth decreased drastically, causing it to plummet to zero. Conversely, the sawing force in the thrust direction decreased to a negative force value and then back to zero during the process. Different parameters may lead to different values, but the variation reflects the fact that with the new trajectory the decrease in depth of cut limits the increase in cutting forces despite the negative rake angle. It should be emphasized that it enables timely chip separation to avoid impact forces, and these increased sawing forces due to the negative rake angle are negligible compared to the impact forces generated in the conventional sawing mechanism ((e.g., force values in Fig. 2).

2.3.2. *Saw teeth arrangement based on new trajectory design*

As shown in Fig. 5c, besides the elliptical-like path on both sides, the intermediate position of the new trajectory is the same as the conventional trajectory, which means that the same ploughing force is introduced, causing wear and deformation of the tooth tips. On the other hand, as described in Fig. 3b, when using the straight edge blade, the intermediate teeth only cut near the extreme. This means that the ploughing force can be partially avoided by the proper arrangement of the tooth tips when using the new trajectory.

As shown in Fig. 8, the trajectory of each tooth tip is related to the arrangement of tooth tips, including the oscillating radius of the tooth tip (R_{T_i}) and the offset angle (ω_i), which denotes the angle between the vertical line and the line connecting the pivot to the i-th tooth tip, and the positive and negative signs of this value represent the direction of deviation (+: right; −: left) [29]. The corresponding trajectory equation can be expressed as

$$P_{New,\,T_i}(t) = \begin{cases} Y(t) = (R_{T_i} - \Delta l_t)\sin(\omega_i + \theta_t) \\ Z(t) = (R_{T_i} - \Delta l_t)\cos(\omega_i + \theta_t) + V_{feed}t \end{cases} \quad (9)$$

The proposed blade edge shape arranges the teeth except for the outermost ones in a concave shape (Fig. 8a), which can effectively reduce the "kicking" phenomenon in surgery [5] and has excellent chip evacuation to avoid clogging [24]. On the contrary, it generates more significant impact force than the straight edge shape due to the considerable depth of the stopped corner when using the conventional oscillating sawing (Fig. 8b). Specifically, this was achieved by adjusting the lateral spacing between adjacent tooth tips, i.e., tooth pitch, and their respective oscillation radii, allowing tooth tip with the smaller oscillation radius to enter the machining area with the larger oscillating radius before moving to point f, i.e., before completing the forward motion, as shown in Fig. 8c. In addition, the positive rake face of the outermost teeth ($T_{L,1}$ and $T_{R,1}$) needs to face outward to avoid the impact force during stopped groove sawing. Since the tips of the two teeth ($T_{L,1}$ and $T_{L,2}$; $T_{R,1}$ and $T_{R,2}$) are oriented in opposite directions, in order to avoid excessive ploughing force on the negative rake face during oscillation, the oscillation radii of them need to be set to the same value in order to minimize the depth of cut, as mentioned in Fig. 3a.

Overall, through the above theoretical analysis, the proposed trajectory can effectively reduce the sawing force, especially the part of impact force and ploughing force which is prone to cause damage to the bone and the blade.

2.4. *Mechanism of the proposed oscillating saw*

To realize the designed trajectory motion, a new oscillating saw mechanism was proposed and filed in a patent, as shown in Fig. 9. Shaft 1 drives the eccentric wheel, causing the oscillating shank to produce oscillation (Fig. 9c, e). Simultaneously, through the gear pair, Shaft 2 drives the cam and roller mechanism, producing an up-and-down movement (Fig. 9d, e). As a result, these two motions couple to achieve the design, creating an elliptical-like path trajectory on both sides of the oscillation. Arcs $\overset{\frown}{AB}$ and $\overset{\frown}{BC}$ are the depression relative to the circular profile, i.e., elliptical-like path generated when the roller contact cam

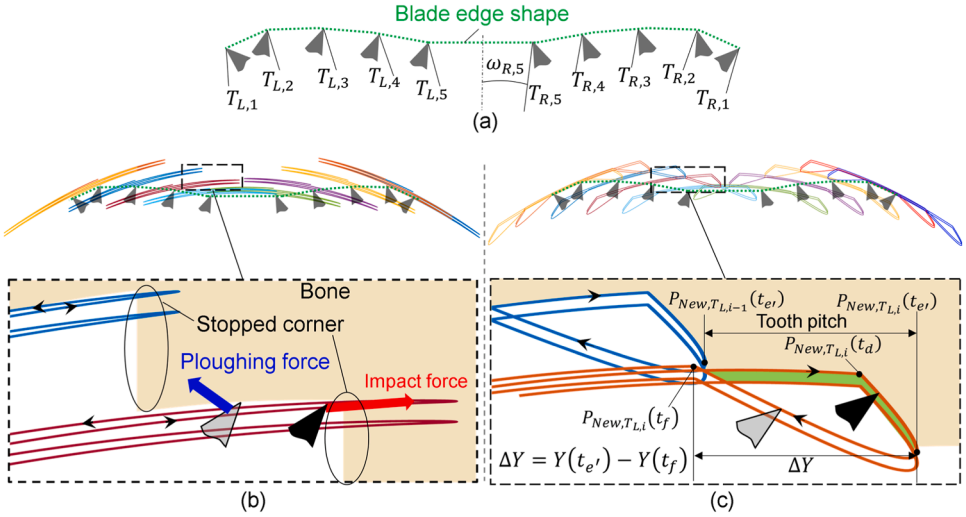

Fig. 8. Optimized saw tooth tip arrangement based on the proposed trajectory. (a) Saw tooth tip arrangement. (b) Conventional trajectory of the saw tooth tips. (c) Proposed trajectory of the saw tooth tips. $T_{L,i}$ and $T_{R,i}$ denote the i-th tooth tip number from the left and right sides to center, respectively. To avoid ploughing force generate at the i-th tooth tip, the distance ΔY (between point f and e' in Y-direction) should be smaller than the tooth pitch, and the point $P_{New,\,T_{i-1}}(t_{e'})$ in Z-direction should larger than that of $P_{New,\,T_i}(t_f)$.

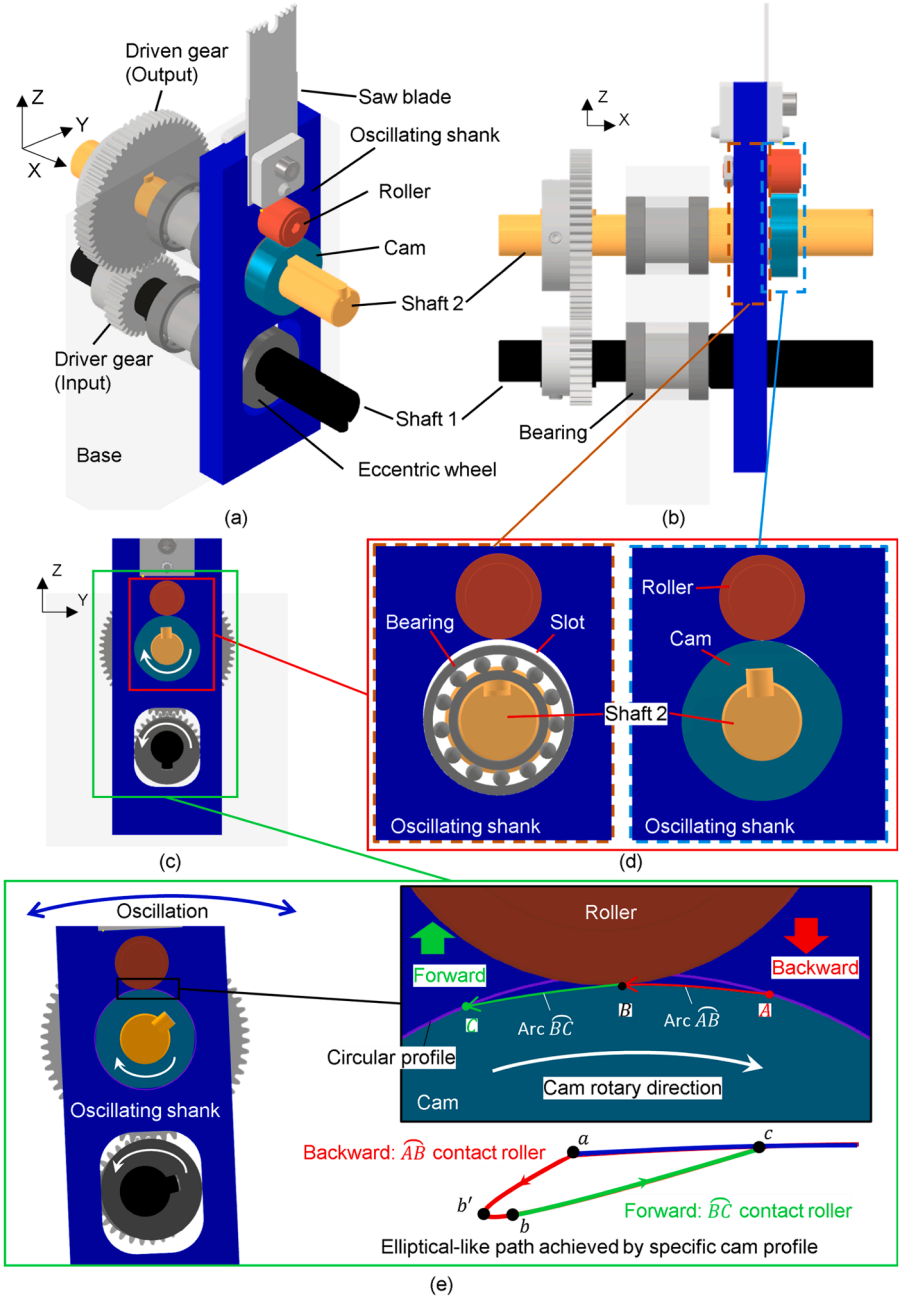

Fig. 9. Proposed oscillating saw mechanism: (a) Isometric view. (b) Side view. (c) Front view. Detail views of (d) cam and roller, and (e) oscillating shank and eccentric wheel. Shaft 1, driven by the motor, drives Shaft 2 via a gear pair (Gear 1 and Gear 2). The eccentric wheel fixed on Shaft 1 drives the oscillating shank and blade, causing them to oscillate around Shaft 2. The cam is fixed on Shaft 2, and the roller, fixed on the oscillating shank, makes contact with the cam profile. A slot, as shown in detail view (d), on the oscillating shank allows Shaft 2 to move up and down, achieved by the roller-cam contact. Backward motion occurs when the cam rotates into the depression relative to the circular profile (Arc $\widehat{A\ B}$), and forward motion occurs when the cam rotates out of the depression relative to the circular profile (Arc $\widehat{B\ C}$). The elliptical-like path results from the combined oscillation and backward-forward motion. All the shafts are supported by bearings and base. A detailed animation of this simulation is available in the supplementary material 1.

profile at the depression (Arc $\widehat{AC}$). On the contrary, when the cam is a profile is circle, there is only oscillation but no up-down motion, the trajectory is become to conventional oscillating sawing trajectory.

To clarify the blade motion trajectory of the newly proposed mechanism, it is essential to establish the relationship between the geometric characteristics of the mechanism and the blade trajectory. As shown in Fig. 10a, the oscillation of the saw blade around the oscillating shaft center (O_2) can be simplified to the O_2Q in motion along the eccentric path of the eccentric wheel (position on the eccentric path: Q, rotary shaft center: O_1, eccentric radius: r_1). Therefore, the instantaneous oscillating angle (θ_t) can be expressed as

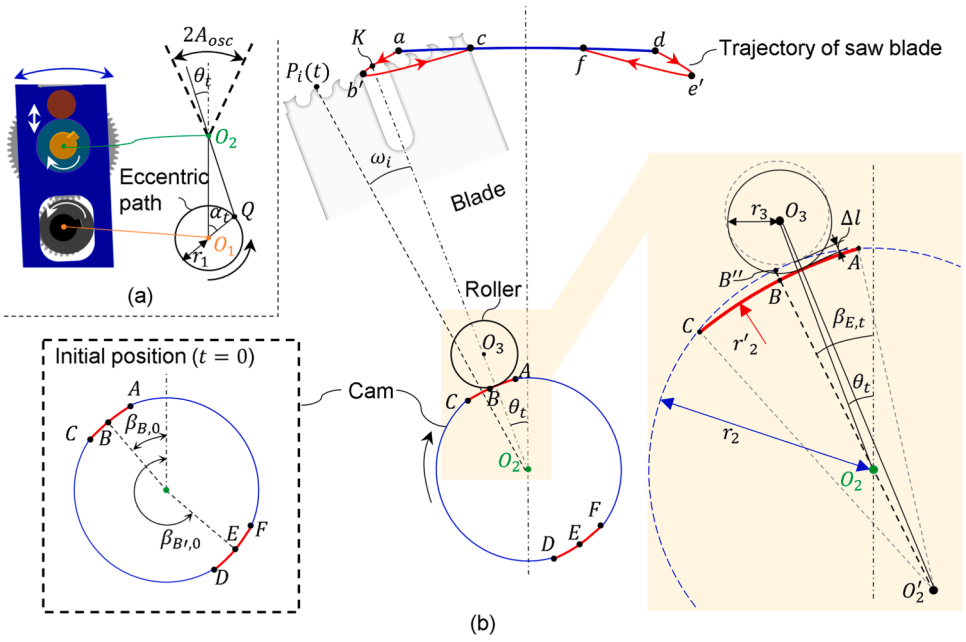

Fig. 10. Geometric characteristics of the proposed mechanism. (a) Relationship between rotary angle (α_t) and oscillating angle (θ_t). (b) Relationship between cam-roller contact and blade trajectory. A detailed animation of cam-roller contact is available in the supplementary material 1.

$$\theta_t = \arccos\left(\frac{\overrightarrow{O_2O_1} \bullet \overrightarrow{O_2Q}}{\|O_2O_1\| \bullet \|O_2Q\|}\right) = \arccos\left(\frac{l_{O_2O_1} - r_1\cos\alpha_t}{\sqrt{(r_1\sin\alpha_t)^2 + (r_1\cos\alpha_t - l_{O_2O_1})^2}}\right) \tag{10}$$

where $l_{O_2O_1}$ is the distance between O_2 and O_1; the rotary angle (α_t) is proportional to the rotational speed (n (rpm)), which can be expressed as

$$\alpha_t = 360 \times \frac{n}{60} t = 6nt \tag{11}$$

As shown in Fig. 10b, the cam profile is separated into different arcs with two different radii. Arcs $\overset{\frown}{C\,D}$ and $\overset{\frown}{A\,F}$ have a radius of r_2, which is smaller than the radius of arcs $\overset{\frown}{A\,C}$ and $\overset{\frown}{D\,F}$ (r'_2). When the compound motion of cam rotation and roller oscillation causes the contact point of the roller and the cam to be at $\overset{\frown}{C\,D}$ and $\overset{\frown}{A\,F}$, the distance between the cam and the roller ($l_{O_2O_3}$) remains constant. While when the contact point enters $\overset{\frown}{A\,C}$ and $\overset{\frown}{D\,F}$, the distance ($l_{O_2O_3}$) varies, leading to a variation in the actual oscillating radius of point P on the blade ($R - \Delta l_t$), which causes the paths $a \rightarrow b \rightarrow c$ and $d \rightarrow e \rightarrow f$ in the proposed trajectory. Therefore, Δl_t can be seen as

$$\Delta l_t = r_2 + r_3 - l_{O_2O_3} \tag{12}$$

where r_3 is the radius of the roller. The value of Δl_t is maximum when the point of contact reaches the midpoint B of $\overset{\frown}{A\,C}$ (or the midpoint E of $\overset{\frown}{D\,F}$), i.e., $\Delta l_t = l_{BB''} = l_{EE'} = C_2$.

According to the cosine theorem of a triangle, $l_{O_3O'_2}$ can be expressed as

$$l^2_{O_3O'_2} = \left(r'_2 + r_3\right)^2 = l^2_{O_2O_3} + l^2_{O_2O'_2} - 2l_{O_2O_3}l_{O_2O'_2}\cos\left(|\theta_t| + \left(180^\circ - \beta_{B,t}\right)\right) \tag{13}$$

where O'_2 is the center of $\overset{\frown}{A\,C}$; $\beta_{B,t}$ is the angle required to rotate point B to the top of the cam, which can be expressed as

$$\beta_{B,t} = \beta_{B,0} - \frac{\alpha_t}{G} \tag{14}$$

where G is the gear ratio; $\beta_{B,0}$ is the initial angle required to rotate point B to the top of the cam. Eqs. (13) and (14) describe the path $a \rightarrow b \rightarrow c$ generated when the blade oscillates on the left side, while the path $d \rightarrow e \rightarrow f$ can be generated by the same manner when it oscillating on the right side, e.g., setting the initial angle required to rotate point E to the top of the cam ($\beta_{E,0}$).

Finally, by substituting Eqs. (10), (11), and (12)–(14) into Eq. (9) and adjusting the appropriate parameters, the desired tooth tips trajectory can be obtained.

3. Experimental verification

3.1. Experimental setup

Comparison experiments were conducted using a setup based on a machining center (AJV-18, Yamazaki Mazak). A self-developed oscillating motion device was fixed on the X-axis table of the machining center (Fig. 11a). This device was driven by a servo motor to oscillate at speeds of 1–6000 CPM (cycles per minute), with an oscillating angle of 5.1° (± 2.55°), achieved by setting the eccentric radius as 2 mm and $l_{O_2O_1}$ (distance between upper and lower shaft) as 45 mm. The conventional oscillating motion and the newly proposed oscillating motion can be switched by assembling the cam of different shapes. The profile of Cam 1 for achieving the conventional oscillating motion is a circle with a radius of 15 mm. The gear pair with gear ratio of 2 to reduce the torque on the upper rotary shaft. Therefore, the profile of Cam 2 for achieving the proposed oscillating motion is combined with 8 arcs as shown in (Fig. 11c).

The typical dimensions of commercial saw blades used in surgery for large bone cutting are 110 mm in length from blade edge to oscillating pivot; 25 mm in width of blade edge and 0.8–2 mm in thickness of blade; 1.3–3 mm of lateral spacing between adjacent teeth; 40–60° of lip angle and −30°–10° of rake angle of saw tooth. Therefore, the saw blades were

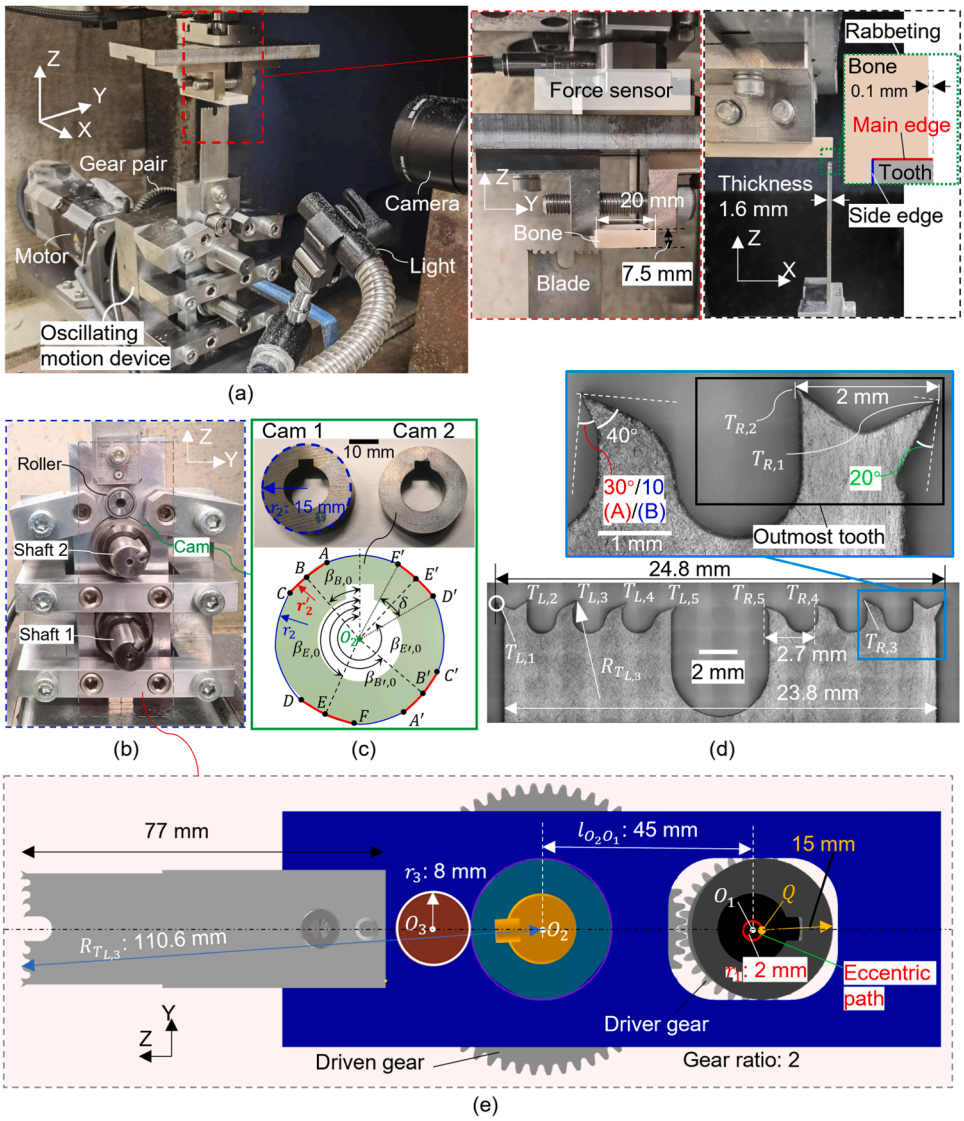

Fig. 11. Experimental setup. (a) Overview of the experimental setup. (b) Front view of the oscillating motion device. (c) Detailed view of Cam1 and Cam 2 for switching between conventional and proposed oscillating sawing mechanisms in the device. (d) Saw blade teeth shape. (e) Dimension of the proposed mechanism. The difference between Blade A and Blade B is the rake angles (30° and 10°) in the teeth except the outermost teeth, i.e., $T_{L,3}$ and $T_{R,3}$, $T_{L,4}$ and $T_{R,4}$, $T_{L,5}$ and $T_{R,5}$. The outermost teeth tips of both blades have the same rake angle (20°) and oscillating radius (110.9 mm).

machined by wire EDM on a stainless steel (JIS SUS440C) plate with dimensions of 77 mm in length to generate similar length from blade edge to oscillating pivot (Shaft 2) with the commercial blade, 25 mm in width, and 1.6 mm in thickness to keep high stiffness and avoid blade bending. The outermost teeth have two tips ($T_{L,1}$ and $T_{L,2}$; $T_{R,1}$ and $T_{R,2}$) with different orientation but same oscillating radius (110.9 mm) and rake angle of 20° (Fig. 11d). The oscillating radius of the remaining teeth is 110.6 ($T_{L,3}$ and $T_{R,3}$), 110.3 ($T_{L,4}$ and $T_{R,4}$), 110 mm ($T_{L,5}$ and $T_{R,5}$) in order of proximity to the outermost tooth with a lateral spacing of 2.7 mm to supply a larger spacing for chip evacuation. Those parameters were selected based on the analyzation of tooth tips trajectories mentioned in Section 2.3.2. To explore the effectiveness of using a large positive rake angle in oscillating sawing, two types of blades (Blade A, Blade B) were used with different rake angles for the tooth tips except the outermost teeth, i.e., $T_{L,3}$ and $T_{R,3}$, $T_{L,4}$ and $T_{R,4}$, $T_{L,5}$ and $T_{R,5}$: 30° and 10°, respectively. The lip angle for each tooth tip was set as 40° to reduce the value of the negative rake angle of each tooth tip. To identify blade damage under the conventional and proposed mechanisms, two sets of blades with those two types (Blade A, Blade B) were used separately in each mechanism. The corresponding values of dimensional parameters of the device (reference Fig. 10 and Fig. 11e) are listed in Table 1. The maximum value of Δl_t was 0.35 mm ($l_{BB''} = r_2 - l_{BO_2}$), which same as in Section 2.3. The consistency of the experimental setup with the trajectories of saw tooth tips presented in Section 2.3 was verified by a 3D model motion simulation using Autodesk Inventor Professional 2024 software. A detailed animation of this simulation can be found in the supplementary material 1.

To enhance the visibility of the sawing process, rabbeting (sawing a groove along the edge of the bone) was utilized in this experiment (Fig. 11a, right side). While this method may differ from actual sawing processes in aspects such as heat dissipation and bone strength, it is still

Table 1
Dimensional parameters of the oscillating motion device.

Design parameters	Values (Unit)
$l_{O_2O_1}$, $l_{O_2O_2'}$, l_{BO_2}	45 (mm), 5.35 (mm), 14.65 (mm)
r_1, r_2, r_2', r_3	1 (mm), 15 (mm), 20 (mm), 8 (mm)
$\beta_{B,0}$, $\beta_{E,0}$, $\beta_{B',0}$, $\beta_{E',0}$	57 (deg), 145.3 (deg), 237 (deg), 325.3 (deg)
δ	48.43 (deg)

suitable for conducting comparative experiments. The cutting thickness was set to 1.5 mm which was smaller than the thickness of the blades (1.6 mm). During sawing, both the main edge and the side edge cut the workpiece simultaneously [29], similar to metal parting, resulting in a combined effect of orthogonal cutting in different directions [16]. The effective cutting width for the main edge was 1.5 mm. The cutting width for the side edge was considered as equal to the instantaneous depth of cut [29], contributing only a small portion of the overall sawing force. Therefore, the difference in sawing forces between different mechanisms can be attributed primarily to the main cutting edge, while the ploughing effect or friction on the machined surface generated by the side edge were ignored for comparison.

A high-speed camera (HAS-EF, DITECT) was used to observe the sawing processes. Cutting forces were measured with a 3-component force sensor (9327 C, Kistler) and collected using a data logger (NR-600, Keyence) with a sampling frequency of 10 kHz (Fig. 11).

3.2. Experimental procedure

The comparative experiments first involved side stopped groove cutting (Fig. 12a), where the right outermost tooth was used to cut the left side of a cortical bone (width: 20 mm), creating a stopped groove with width of 4 mm and depth of 2.5 mm, to evaluate the effectiveness of both the conventional and newly proposed oscillating sawing mechanisms in suppressing impact force and ploughing force during stopped grooving. Secondly, the through groove cutting (Fig. 12b) was performed on a cortical bone (width: 20 mm) to compare the differences between the two mechanisms when using the middle teeth (Blade A and Blade B) to cut the workpiece. A single feed of 3 mm (effective cutting distance: 2.5 mm) was used in both experiments for cutting cortical bone. The thickness of the cortical bone sample was 7.5 millimeters, which means that after 3 feeding processes, the machined area was through in the feed direction. Only the force data of the first feeding process was used for comparison due to the relatively stable strength at a shallow feed depth.

The workpieces of cortical bone were taken from the mid-diaphysis of fresh bovine femurs, and the cutting direction was chosen across the osteon direction to mimic the general sawing process.

Lastly, the stopped groove cutting (Fig. 12c) was performed on a simulated cancellous bone (width: 40 mm, made from solid rigid polyurethane foam, SAW1522–27, Sawbones) to mimic the two mechanisms cutting a stopped groove the cancellous bone with a large feed (20 mm). The cutting conditions were listed in Table 2. The oscillating range is the ideal maximum cutting width of the blade in the Y-axis and was calculated as 34.5 mm. The oscillation speed was set as 600 CPM to observe the cutting process clearly and avoid large noise during force data acquisition. In surgery, the surgeon adjusts the feed speed based on the resistance, e.g., using a lower feed speed to cut the harder bone (e.g., cortical bone) to avoid the thin saw blade be bent, and a higher feed speed to cut softer bone (e.g., cancellous bone) to reduce operating time. Therefore, the feed speed was set at 6 mm/min for cortical bone cutting to achieve a depth of 10 μm per oscillating cycle and 12 mm/min for cancellous bone cutting to achieve a depth of 20 μm per oscillating cycle, mimicking the cutting depth used in bone cutting surgery.

Table 2
Cutting conditions.

Workpieces	Bovine cortical bone, width: 20 mm, thickness: 7.5 mm
	Simulated cancellous bone, width: 40 mm, thickness: 30 mm
Blade width, thickness	24.8 mm, 1.6 mm
Oscillating range	34.5 mm
Oscillation speed	600 CPM
Cutting distance	3 mm (cortical); 20 mm (cancellous)
Blade feed speed	6 mm/min (cortical); 12 mm/min (cancellous)
Depth per oscillating cycle	10 μm (cortical); 20 μm (cancellous)

To distinguish between machined and unmachined areas, the side surface of the workpieces, viewed by the camera, was blackened with a black marker in advance.

4. Results and discussion

4.1. Sawing force and machined area

4.1.1. Side stopped groove cut

The use of outermost tooth for the side groove cutting experiment represents the most direct method of comparing the conventional and newly proposed oscillating sawing mechanisms in terms of reducing impact forces. The performance of the newly proposed mechanism can be demonstrated by the cutting force (Fig. 13) and the resulting corner profile after cutting (Fig. 14), showing significant differences compared to the conventional mechanism. In addition, a video recording of the side stopped groove cutting process using both the conventional and proposed mechanisms has been uploaded as supplementary material 2.

Since the raw force data oscillates with the cutting cycle, the peak values of the cutting forces for each oscillating cycle were used for comparison (Fig. 13). With the conventional oscillating sawing mechanism, although the thrust force remains relatively stable with a mean value of 35 N, the cutting force gradually increases during feed, peaking at a maximum of 213 N (Fig. 13a). The large cutting force was due to the large portion of the impact force. The negative cutting force was caused by the ploughing force when the flank of the tooth tip contacted the workpiece during oscillation from right to left, with a mean value of 13 N.

In contrast, the proposed oscillating sawing mechanism significantly reduces the cutting force, stabilizing at a mean value of 34 N throughout the feed (Fig. 13b). The mean value of the negative cutting force was 9 N, which was lower than that generated by the conventional mechanism. It indicates that the new oscillating sawing mechanism effectively reduces the ploughing force of the outermost tooth as expected, compared to the conventional oscillating sawing mechanism.

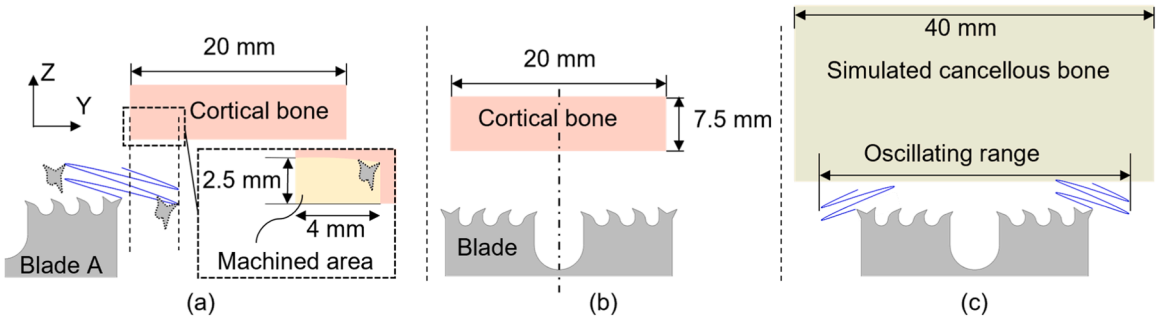

Fig. 12. Oscillating sawing experiments. (a) Side stopped groove cut. (b) Through groove cut. (c) Stopped groove cut.

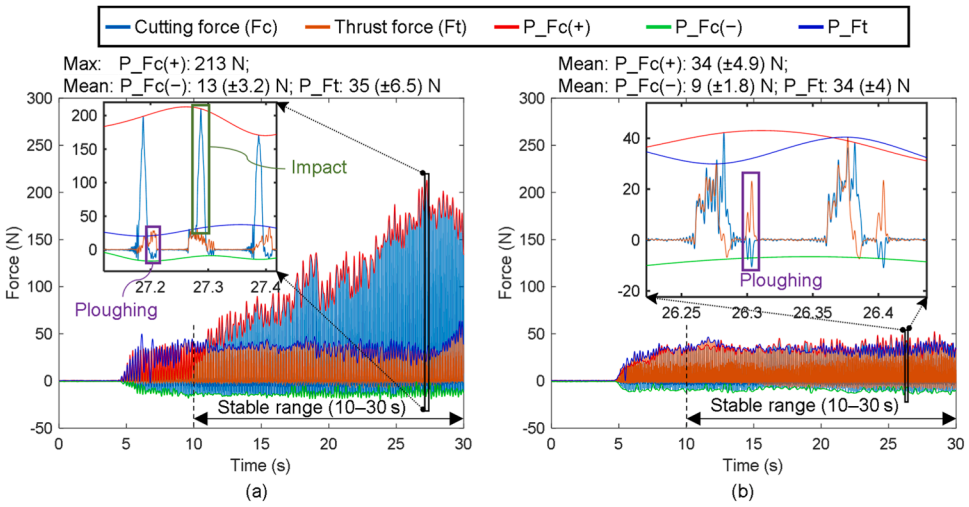

Fig. 13. Comparison of sawing forces in the side groove cutting experiment. (a) Conventional mechanism. (b) Proposed mechanism. The peaks (P_Fc(+), P_Fc(−) and P_Ft) were determined from the envelopes of the force data. The mean forces (mean ±1 standard deviation) were computed within a stable range (10–30 s) for analysis. Experimental conditions: 600 CPM, 6 mm/min, cortical bone.

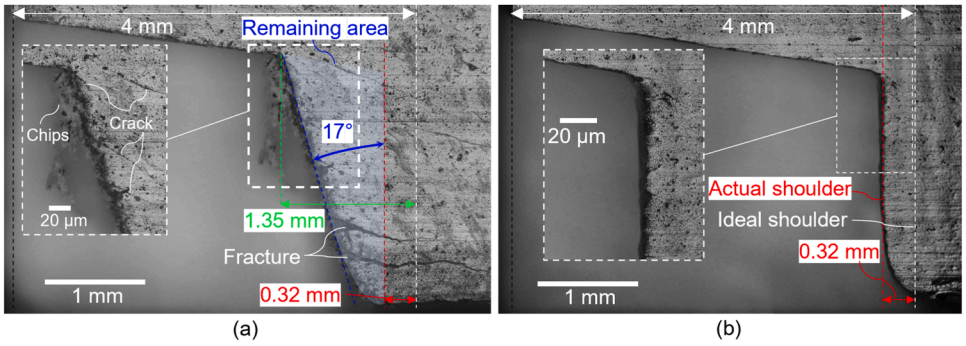

Fig. 14. Comparison of corner profiles after side groove cutting experiments. (a) Conventional mechanism. (b) Proposed mechanism. Experimental conditions: 600 CPM, 6 mm/min feed rate, cortical bone.

From the corner profile of the workpiece machined by the proposed oscillating sawing mechanism (Fig. 14b), it was observed that the actual shoulder profile of the machined side groove (represented by the red dot line) exhibits a slight lateral offset of 0.32 mm from the ideal shoulder position (represented by the white dot line) when using the proposed oscillating mechanism. This small offset may arise from the assembly clearance of the overall experimental system (e.g., the fixture that clamps the bone and the oscillating mechanism). In addition, there was no crack near the shoulder position due to the small impact force being effectively avoided. In contrast, when machining with the conventional oscillating sawing mechanism, a significant angular deviation of the shoulder position occurred (17°), leading to a serious offset of 1.35 mm between the final corner position and the ideal position. This issue caused by the inefficiency of cutting off the workpiece near the extreme of oscillation by the conventional sawing mechanism, resulting in a gradual reduction in the oscillation range of the cutting tip and thereby increasing a remaining area on the workpiece that was supposed to be cut off (excludes the part caused solely by the assembly clearance of the experimental system) (Fig. 14a). This remaining area continuously absorbs impacts from the oscillating saw blade tip, resulting in elastic deformation and inducing crack propagation near the shoulder, especially at the weaker edge positions of the workpiece, which are more prone to fracture.

4.1.2. *Through groove cut*

In the through groove cutting experiment, the cutting force generated by the conventional oscillating sawing mechanism gradually increases with the feed and stabilizes after a certain period (increasing from 5 s and stabilizing from 15 s), as shown in Fig. 15a, b. Although a larger positive rake angle setting can reduce the sawing force, a significant amount of impact force still occurs when using the conventional oscillating sawing mechanism. In addition, obvious defects were present on the edge of the machined surface due to fractures caused by the high impact force and the low strength of the outer layer of the bone (Fig. 16a,b).

On the contrary, as shown in Fig. 15c, d, the proposed oscillating sawing mechanism achieves stability in cutting force more rapidly (increasing from 5 s and stabilizing from 10 s), with the cutting forces consistently lower than those of conventional mechanism. Furthermore, the larger rake angle further contributes to reduced cutting forces. The proposed mechanism caused large sawing force reductions compared with the conventional results: cutting force: 66 % (Rake angle: 10°), 61 % (Rake angle: 30°); thrust force: 57 % (Rake angle: 10°), 39 % (Rake angle: 30°). Therefore, it results in a very smaller proportion of defects compared to the conventional oscillating sawing mechanism (Fig. 16c, d). On the other hand, the ploughing effect has been observed in the machined surface machined by both mechanisms (Fig. 16c,d). The machined surfaces were machined by the side cutting edge of the saw teeth (Fig. 11a, right side). Due to the flat shape of the saw tooth, the rake angle of the side cutting edge can be considered a zero-rake, which ploughs the machined surface while oscillating. Therefore, the differences in the machined surface, except for defects on the bone edges,

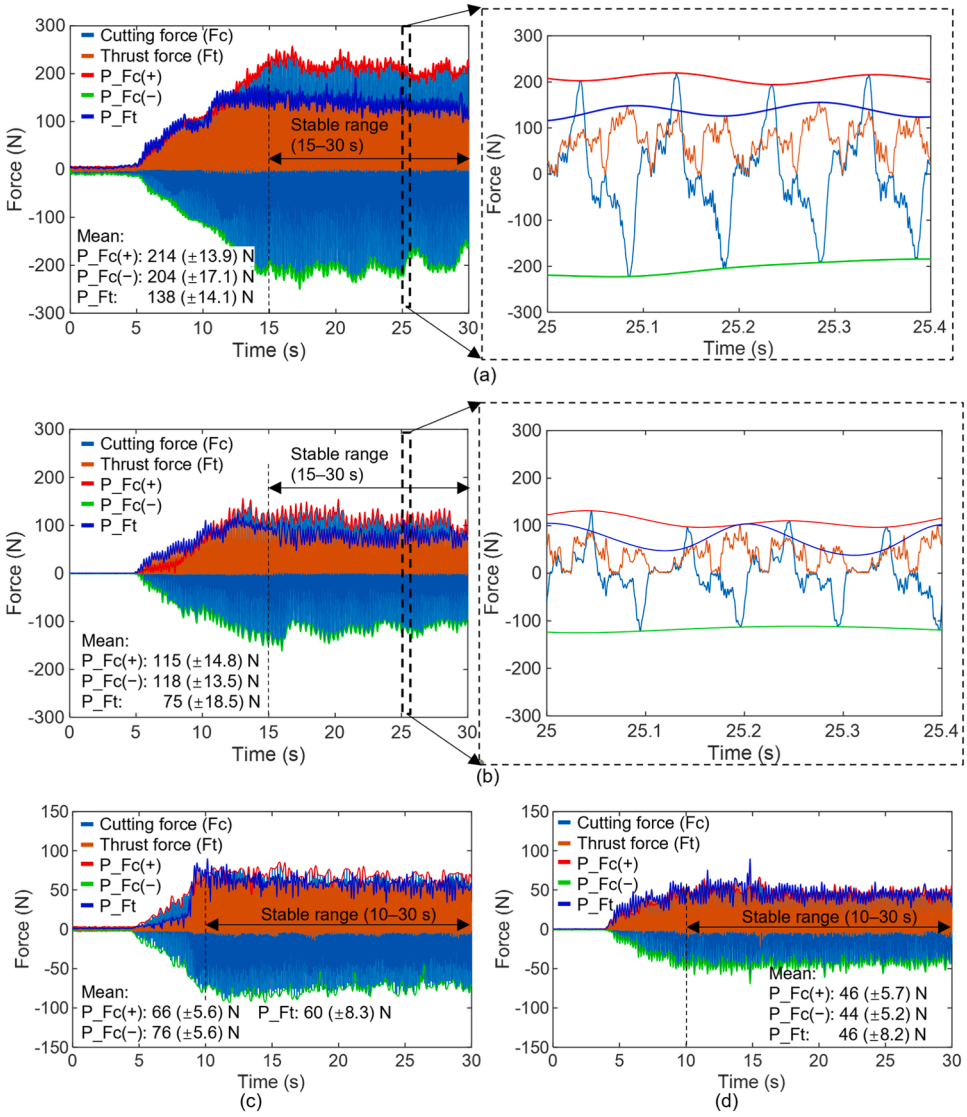

Fig. 15. Comparison of sawing forces in the through groove cutting experiment. (a) Conventional mechanism, rake angle: 10°. (b) Conventional mechanism, rake angle: 30°. (c) Proposed mechanism, rake angle: 10°. (d) Proposed mechanism, rake angle: 30°. Experimental conditions: 600 CPM, 6 mm/min, cortical bone.

were not discussed. Through groove cutting process using both the conventional and proposed mechanisms was recorded in a video, which is provided as supplementary material 3.

4.1.3. *Stopped groove cut*

In experiments involving stopped groove cutting, when the cancellous bone was used, the thrust force was very small but significant cutting force was still generated by the conventional oscillating sawing mechanism, with most part of these forces being stemmed from impact between workpiece and blade (Fig. 17a). This impact force resulted in curved shoulder profiles after sawing. The oscillation range was minimized at a feed rate of 5 mm (30.4 mm) and then gradually recovered (Fig. 17b). This was because during the feeding process, the point of impact was shifted part from the tooth tips to the blade shank upon contact with the curved shoulder, altering the point of impact and thereby reducing the elastic deformation of the saw blade.

In contrast, as shown in Fig. 17c, the proposed oscillating sawing mechanism rapidly stabilizes the cutting force at a low value, achieving an 85 % reduction in cutting force and a 23 % reduction in thrust force compared to the conventional mechanism. The vertical shoulder profile as shown in Fig. 17d further illustrated that the proposed mechanism effectively avoided the impact force generated by the contact between the tooth tip and shoulder.

Looking at the conventional oscillating sawing mechanism from another perspective, even with just one tooth cutting (in Section 4.1.1) or when cutting softer, cancellous bone, such significant forces were still generated. This can well explain why kicking out or grabbing phenomena often occur during actual surgical procedures.

In the side stopped groove cutting, where only one side of the saw blade experiences impact force, it becomes challenging for surgeons to maintain rigidity similar to machine and avoid deviations, leading to the blade being kicked out from the bone. In stopped groove cutting, where both sides of the saw blade are impacted simultaneously, the actual cutting force was substantial but with minimal variation in thrust direction. This can lead to incorrect judgments by surgeons or robotic systems based on thrust force, resulting in grabbing phenomena where the oscillation range gradually decreases or even causing the drive motor to stall.

Currently, most bone cutting studies often use robust young bovine cortical bones aiming to maintain consistent cutting condition, which may significantly differ from the actual surgical scenario. Patients undergoing orthopedic surgeries, e.g., TKA, are typically in elderly patients above 65 years of age [38]. Elderly patients often have bones that are more brittle and susceptible to cracking or fracturing, and they may

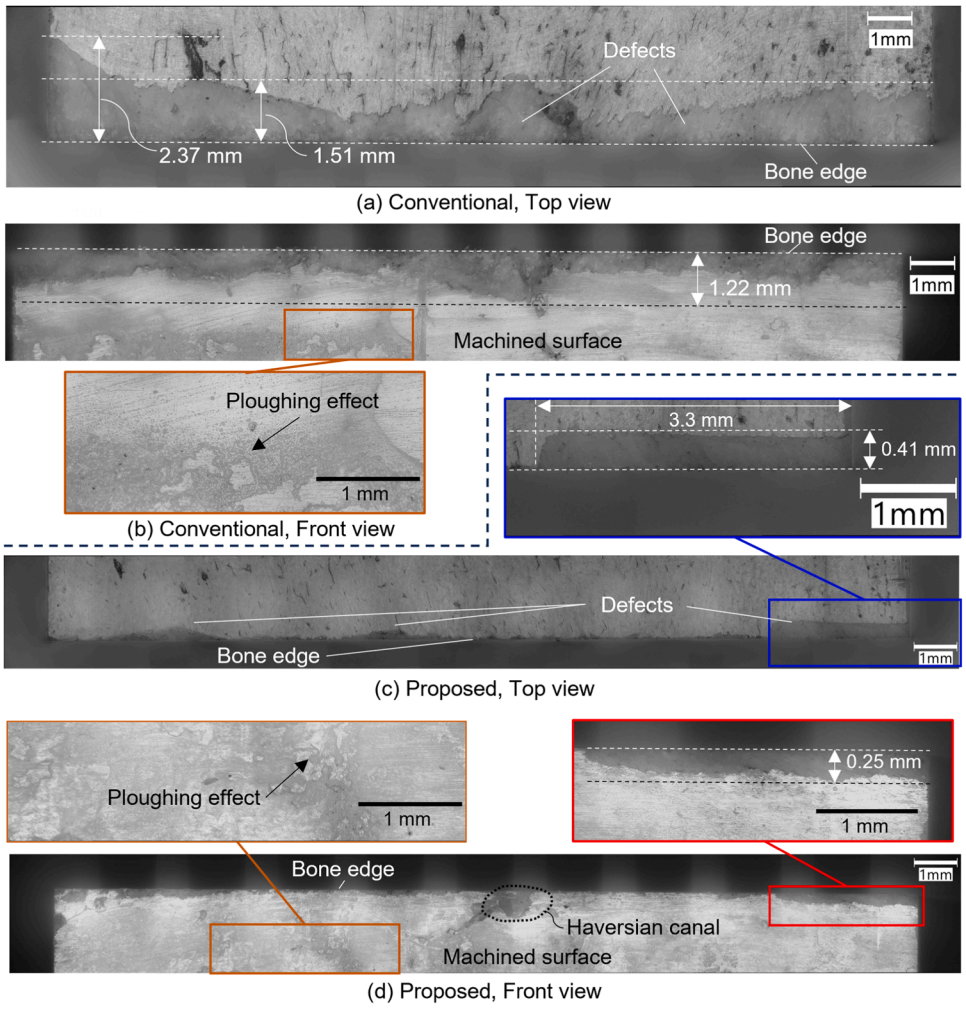

Fig. 16. Defects on the machined surface after the through groove cutting. (a, b) Conventional mechanism. (c, d) Proposed mechanism. Experimental conditions: 600 CPM, 6 mm/min, Blade A, cortical bone (30 mm width). Defects on the bone edge are observed in the supplementary material 3.

experience slower bone recovery post-fracture [39]. Therefore, the impact forces generated during surgeries may be less than those measured in current experiments. However, on the other hand, the defects and fractures caused by impact forces produced by conventional oscillating sawing mechanisms could be more significant than observed in experiments, greatly hindering postoperative recovery for patients. The development of robot-assisted techniques in bone cutting surgeries is rapidly advancing, with major surgical systems still relying on the conventional oscillating saw mechanism [40]. To ensure high blade rigidity, thicker blades are often used, accompanied by the expectation of reduced sawing forces to minimize blade width. However, this setting is more prone to forming stopped groove cutting scenarios, and exponentially increasing the blade thickness will likewise exponentially increase the impact force.

4.2. Saw tooth deformation and wear

Medical saw blades are typically disposable, meaning they are designed for single use. However, there are also reusable saw blades that have stricter requirements for suppressing deformation and wear of the tooth tips. On the other hand, even if the saw blade is single use, this still poses a risk to the patient if the saw teeth is deformed at shorter feed distances, especially when multiple planes of resection are performed during TKA. Therefore, it is necessary to evaluate the deformation and wear of the saw teeth at short feed distances and the effect on the sawing force.

Fig. 18 shows the worn distance of each tooth tip after performing the cortical bone cutting experiments, including one time for the side stopped groove cutting experiments by using the right outermost tooth (only Blade A) as described in Section 4.1.1 (total feed distance: 2.5 mm) and four times of through groove cutting experiments as described in Section 4.1.2 (total feed distance: 30 mm (4 × 7.5 mm)).

The worst deformation of $T_{R,1}$ in Blade A by using the conventional mechanism (worn distance: 0.72 mm, as shown in Fig. 18a) was due to the excessive impact force in the side stopped groove cut. On the contrary, the proposed mechanism caused a smaller deformation at the same tip position (worn distance: 0.08 mm), caused by ploughing force rather than impact.

For all other parts of the tooth, severe deformation occurred under the conventional mechanism, including ploughing force-induced flipping of the tooth tip to the positive rake face, and impact force-induced flipping of the tooth tip to the negative rake face. When discussing the effects of different rake angles (ignoring the deformation of the outermost teeth), although a larger rake angle has a smaller worn distance, it causes more deformation due to ploughing. Specifically, the total worn distance ratio between impact-induced and ploughing-induced deformation increased from 0.2 (Blade B) to 1.67 (Blade A). This suggests that a larger rake angle in the conventional mechanism is not effective in reducing saw tooth deformation.

On the other hand, small tooth deformation and wear occurred under the proposed mechanism, which mainly included dulling of the edge by wear and ploughing force-induced deformation, especially when using

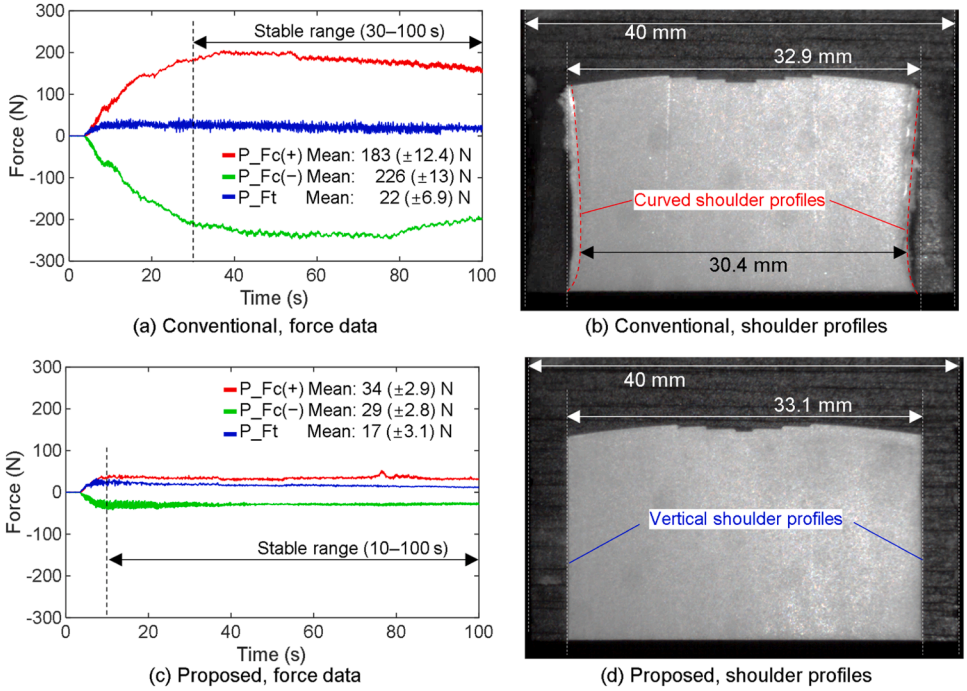

Fig. 17. Comparison of sawing forces during the stopped groove cutting experiment. (a, b) Conventional mechanism. (c, d) Proposed mechanism. Force reduction ratio: 85 % (cutting force); 23 % (thrust force). Experimental conditions: 600 CPM, 12 mm/min, rake angle: 30°, simulated cancellous bone (40 mm width), feed distance: 20 mm.

Blade A, which has a large rake angle (30°) in the teeth except the outermost ones. These wear and deformations may be caused by deviations from the ideal trajectory due to the assembly clearance of the whole system, as mentioned in Section 4.1.1. Additionally, defects in the tooth tips resulting from machining with wire EDM may also promote wear and deformation at small worn distances. The average worn distance in both Blade A and Blade B caused by the proposed mechanism was around one-tenth of that produced by the conventional mechanism.

Fig. 19 shows that severe deformation when using the conventional mechanism caused the cutting force to increase significantly with the feed distance. Although a large rake angle can reduce the wear distance of the saw teeth and consequently reduce the increased sawing force due to teeth deformation, the force increase was still much higher compared to using the proposed mechanism. In contrast, the blades used with the proposed oscillating sawing mechanism consistently generated similar cutting forces during each experimental time, especially when using Blade A with the larger rake angle.

The experimental results indicate that using the proposed oscillating sawing mechanism can effectively improve saw teeth wear conditions and enable the setting of a large positive rake angle on the saw blade teeth. By effectively avoiding contact with negative rake angles, setting a larger lip angle increases the strength of the tooth tips. This approach helps reduce the risk of tooth tip deformation and fracture, ensuring that during the surgical process, the tooth tips can efficiently cut bone with smaller, more stable forces, thereby reducing the risk of metal residues caused complications.

4.3. *Evaluation and outlook of the proposed oscillating sawing mechanism*

4.3.1. *Discussion with elliptical vibration cutting path*

The proposed oscillating sawing mechanism employs an elliptical-like trajectory at the extremes of oscillation, which exhibits similarities and differences compared to paths used in elliptical vibration cutting techniques. Elliptical vibration cutting techniques have been widely utilized in precision machining [41], and their typical cutting path is illustrated in Fig. 20a [42]. The combination of elliptical motion and the feed motion in cutting direction involves the tool first removing the workpiece material and then separating from it within each vibration cycle. This intermittent cutting process, accompanied by the reversal of friction between the rake face and the workpiece, leads to a significant reduction in cutting forces [42,43]. Similarly, the intermittent contact with the workpiece during the oscillating sawing process reduces sawing forces by avoiding contact with the workpiece at a negative rake angle in the proposed trajectory (Fig. 20b). In a single oscillating sawing cycle, the direction of its elliptical-like trajectory aligns with that of elliptical vibration cutting technology. However, when viewed from the overall feed direction, it is opposite to the direction used in elliptical vibration cutting technology. This design aims to achieve smaller cutting depths at the point of contact with the workpiece and avoid negative rake angle, thereby facilitating chip separation from the workpiece. On the other hand, the amplitude of the elliptical trajectory component in the proposed trajectory is much larger than that used in elliptical vibration cutting. Although vibration cutting technology can promote chip separation from the workpiece through crack propagation [7], the effectiveness of this process in separating chips from the workpiece at the extremes of oscillation during stopped groove cutting remains uncertain, especially considering the elastic recovery of cortical bone at small depths of cut [25] and assembly clearance (as mentioned in Section 4.1.1).

4.3.2. *Temperature rise*

Although this study did not measure temperature rise, the temperature rise in orthogonal cutting and oscillating sawing experiments in this research can be discussed through previous studies.

The temperature increase from conventional bone sawing can reach 100 °C in the localized cutting region [9], potentially causing thermal and mechanical damage to the bone [11]. While clinical conditions may vary due to interstitial fluid in natural bone, particularly cancellous bone [44], the rise in temperature during the sawing process remains a significant concern, which includes risks such as chip clogging [24] and the absence or less effectiveness of a cooling process as depth increase of the stopped groove.

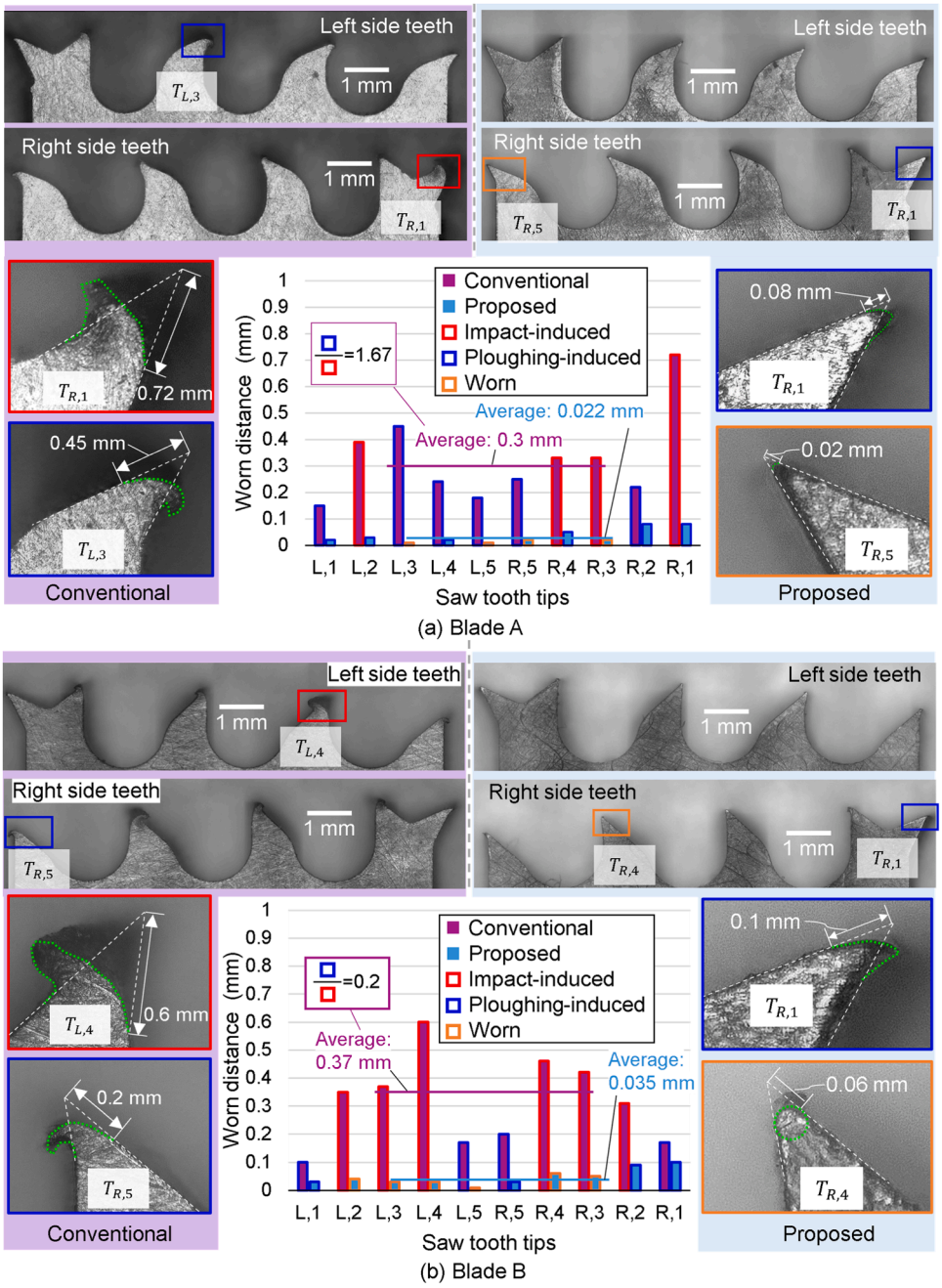

Fig. 18. Deformation and wear with the worn distance of each tooth on (a) Blade A and (b) Blade B. Worn distance: distance between the ideal cutting edge and the undeformed position on the rake face. Deformation types: impact-induced: tooth tip flipping towards the negative rake face; ploughing-induced: tooth tip flipping towards the positive rake face; worn: no obvious flipping of tooth tip. Average worn distance (± 1 standard deviation) for teeth except the outermost teeth: Blade A: 0.3 (±0.09) mm (conventional), 0.022 (±0.01) mm (proposed); Blade B: 0.37 (±0.16) mm (conventional), 0.035 (±0.02) mm (proposed). Total worn distance ratio between ploughing-induced and impact-induced deformation for conventional mechanism: Blade A: 1.67; Blade B: 0.2. Total feed distance before measurement: 2.5 mm (side stopped groove), 30 mm (through groove).

The temperature rise is primarily determined by the difference between the heat generated and dissipated within the system per unit of time. In orthogonal cutting experiments, heat is generated from the shear cracks on the chip shear plane, friction between the chips and the rake face, and friction between the workpiece and the cutting edge and flank [19,27]. Feldmann et al. [19] observed that during orthogonal cutting experiments on cortical bone with a positive rake angle, the primary heat concentration occurs on the chips, followed by the rake face of the cutting tool, and lastly on the workpiece surface. This result indicates that the temperature rise is minimal if the chips are promptly removed.

When using a negative rake angle for cutting, a significant amount of frictional heat generated during the ploughing process transfers to the workpiece surface and the rake face [45], as only a small amount of chips is produced [25]. Therefore, larger negative rake angles often result in more significant heat accumulation in the machining area if it is not promptly dissipated. On the other hand, impact forces can also generate substantial heat. Repeated impact forces during oscillation can be considered cyclic loading, which induces microcracks in the bone [46] (Fig. 14, supplementary material 2). These microcracks absorb energy through sliding mechanisms within and between fibrils [47], potentially resulting in frictional heat [48]. The heat is not dissipated

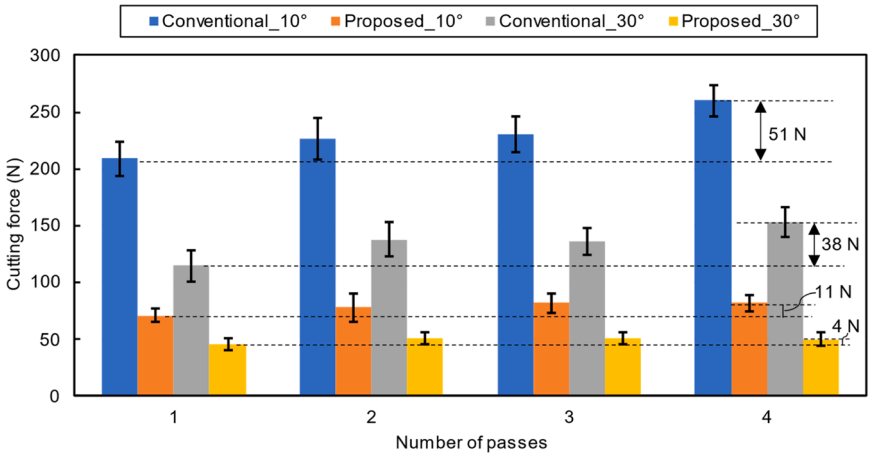

Fig. 19. Variation in cutting force with the number of passes (through groove cutting experiment in **Section 4.1.2**). Feed distance: Pass 1: 2.5 mm; Pass 2: 10 mm; Pass 3: 17.5 mm; Pass 4: 25 mm. Error bars represent ±1 standard deviation for the mean cutting force values calculated within a stable range, as mentioned in Fig. 13.

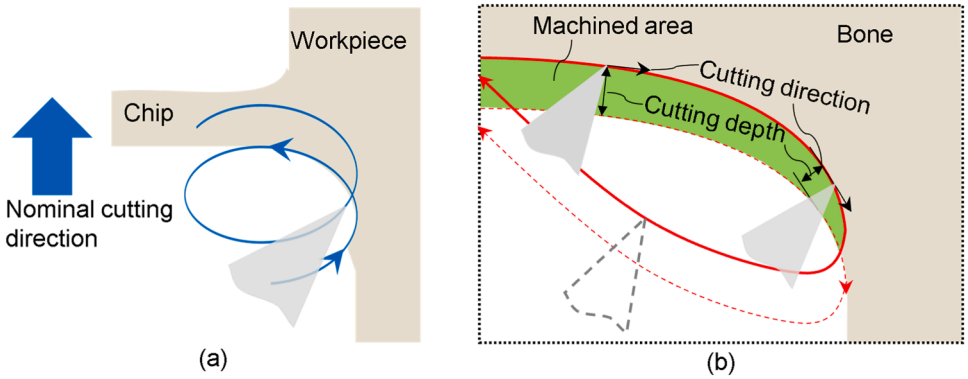

Fig. 20. Elliptical paths in elliptical vibration and proposed sawing. (a) Elliptical vibration cutting path [42]. (b) Elliptical-like path near the extremes of oscillation of the proposed trajectory design (described in Section 2.2).

through chip removal but spreads within the bone, causing a temperature rise in the machining area. Similarly, the temperature rise due to repeated impacts is evident in ultrasonic vibration cutting processes, including heat generated by flank face crushing during drilling [49] and bone tissue burns due to large thrust forces in sawing [34].

As shown in Fig. 21a, even using the positive rake angle, it was difficult for the conventional sawing mechanism to separate the chips from the stopped corner, which caused the chips to accumulate in the corner and the heat within the chips to accumulate in the machining area. In addition, it will spread to the saw teeth and workpiece during oscillation, resulting in a significant temperature rise. Furthermore, the accumulated chips may prevent new chip formation and evacuation, thus increasing the risk of chip clogging, which further increases the temperature rise and sawing force.

In contrast, the proposed mechanism effectively separates chips from the workpiece, enhancing heat dissipation capability (Fig. 21b). Furthermore, the proposed mechanism also reduces heat generation by effectively avoiding impact forces and reducing ploughing forces—two force components that do not contribute to chip removal. Although the actual rake angle of the teeth changes to negative during backward motion, the decreased cutting depth avoids large heat generation. These combined improvements indicate that the proposed mechanism should produce a lower temperature rise than the conventional one. Additionally, considering that conventional sawing mechanisms often lead to increased blade tooth wear and deformation during the sawing process, the new mechanism's ability to minimize these issues further highlights its effectiveness in mitigating temperature rise.

From a single-chip formation perspective, the difference in the morphology of the chips produced by these two mechanisms was primary the thickness of the end of the chips, as shown in Fig. 22. The end of the chip produced by the conventional mechanism was thicker because the instantaneous depth of cut was maximized (Fig. 22a). In contrast, the end of the chip produced by the proposed mechanism was as thin as expected, thus facilitating separation from the workpiece (Fig. 22b). It should be mentioned that the end of the chip produced by the conventional mechanism should be less than the ideal thickness because a portion of the chip was not removed, resulting in an inclined shoulder as described Fig. 14a.

The chips generated through the proposed mechanism are consistent with the general cortical bone chip formation mechanism in orthogonal cutting experiments, i.e., continuous serrated chips at a small cutting depth [18,25,50]. However, the end part of the chips shows an increased tendency for local separation (Fig. 22b). This was due to the reduction in the depth of cut and the variation of the rake angle from positive to negative. The continuous chip may increase the risk of chip clogging during evacuation, particularly with larger cutting depths per cycle, necessitating additional blade design considerations for chip evacuation in the future. In addition, recent studies have shown that during ultrasonic vibration-assisted cutting of cortical bone, chips become semi-continuous or discontinuous chips due to more fractures inside the chips caused by high-speed vibration, which may also promote the further decomposition of chips and thus facilitate chip evacuation [51].

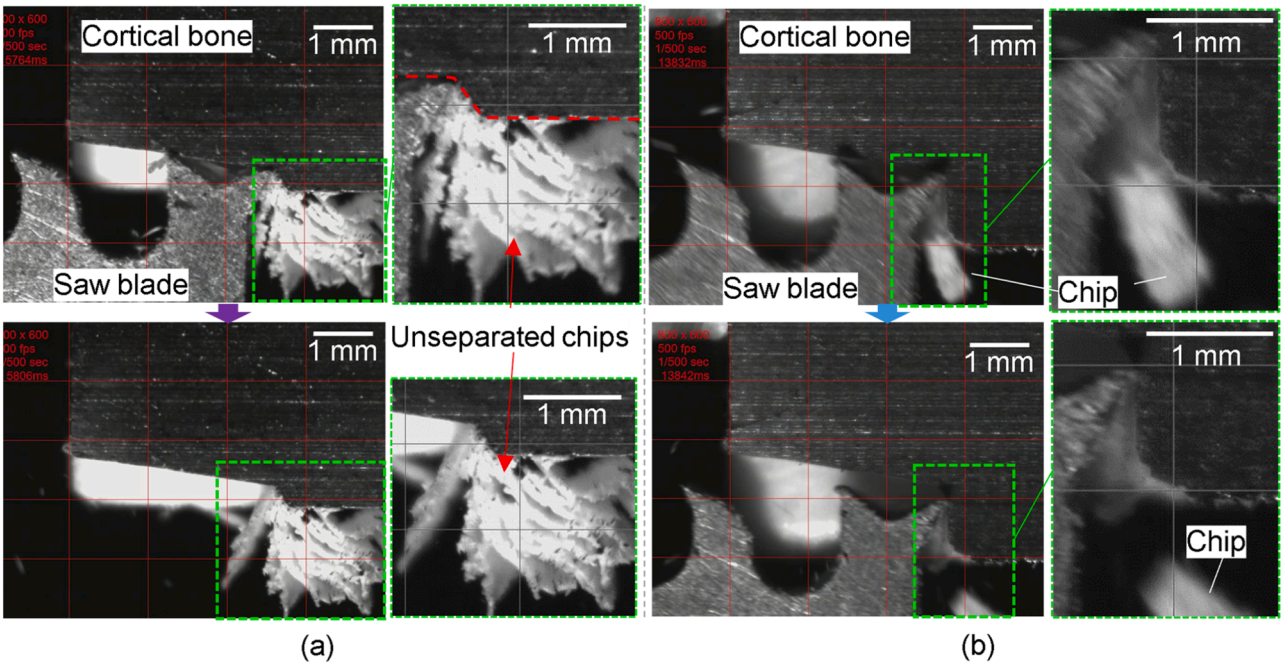

Fig. 21. Bone chips in the side stopped groove cutting process. (a) Conventional mechanism. (b) Proposed mechanism. Video recording is available in the supplementary material 2.

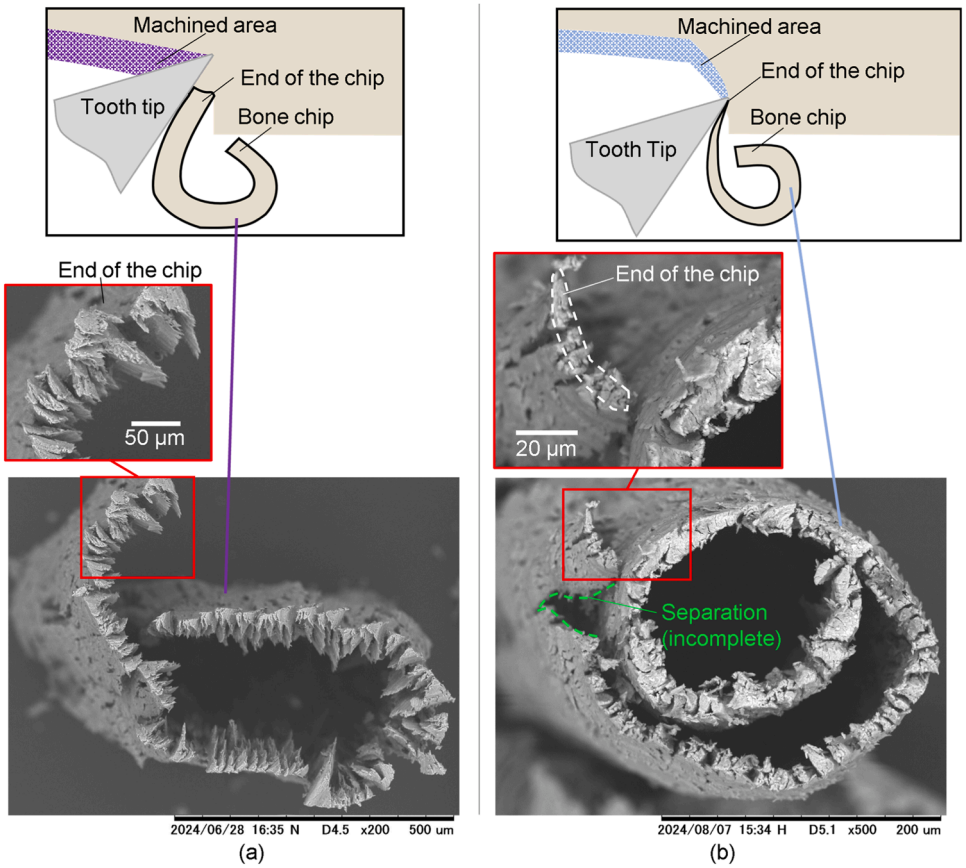

Fig. 22. Side view of the bone chips generated in the side stopped groove cutting experiments. (a) Conventional mechanism. (b) Proposed mechanism.

4.3.3. Challenges and future directions for surgical prototype

The proposed mechanical structure validates the effectiveness of trajectory and blade edge designs in reducing oscillating sawing forces and saw teeth deformation, particularly addressing impact and ploughing forces. It also allows for utilizing saw teeth with larger rake angles to increase cutting efficiency. However, it is important to

acknowledge that further considerations and validations are necessary before clinical application.

During surgical procedures, the oscillating saw operates at high oscillating speeds with a compact mechanical structure for handheld control. Incorporating additional forward/backward motion may require enhanced design considerations to effectively accommodate these high oscillation speeds and handheld control requirements.

Furthermore, the current parameters have not been fully optimized, necessitating future optimization to achieve the best clinical cutting outcomes. This includes exploring optimal parameters for rake angles and other design features to enhance performance in varying surgical conditions.

Moreover, while the design with larger rake angles has shown promise at the small cutting depths, the potential risks associated with larger cutting depths, such as tooth tip fractures or deformations, necessitate more comprehensive comparative experiments for thorough exploration. Effective strategies should be proposed to mitigate these risks effectively.

4.3.4. Potential field for exploitation of the proposed cutting mechanism

Although oscillating sawing technology has been widely used in bone cutting surgery and extensively in the home improvement industry as a versatile handheld tool (known as an oscillating multi-tool), its application in precision machining has been limited. However, this sawing technique holds potential as a method for processing thin deep groove cuts if its sawing forces and blade wear can be significantly reduced. Currently, machining thin and deep grooves often requires drilling multiple holes using micro-drills or employing processes such as electrical discharge machining (EDM), for instance, when machining seal slots for turbomachinery [52]. However, these methods present challenges in terms of tool wear and processing time due to the narrow and deep nature of the grooves. The proposed oscillating sawing mechanism, when used for cutting bone in stopped groove operations, essentially performs thin deep groove cutting. Given these capabilities, there is potential for oscillating saw technology to inspire new approaches in precision machining. By reducing sawing forces and blade wear, oscillating saws could offer an efficient alternative for machining thin and deep grooves, potentially overcoming the limitations associated with existing methods such as micro-drilling and EDM. In summary, while oscillating saw technology has not traditionally been associated with precision machining, the proposed oscillating sawing mechanism demonstrated effectiveness in bone cutting surgeries suggests promising applications in this field. Further research and development are needed to optimize this technology for precision machining tasks, potentially enabling faster and more efficient processing of thin deep grooves.

5. Conclusions

In this study, an innovative oscillating saw mechanism was proposed based on a comprehensive analysis of tooth tip trajectories to reduce sawing forces, particularly impact force and ploughing force that did not contribute to chip formation. A method was introduced to incorporate a reverse feed motion near the extremes of oscillation, altering the cutting depth and rake angle of the tooth tip to break off continuous chips from the workpiece, thereby avoiding the accumulation of impact force. Additionally, saw blade tooth tip positions aligned according to the proposed motion trajectory to avoid contact between the negative rake face of the tooth tips and the workpiece, reducing ploughing force. The bone cutting comparison experiment with conventional oscillating sawing mechanisms demonstrated the excellent performance of the newly designed oscillating sawing mechanism, showing significant reductions in impact and ploughing forces, thus avoidance of cracks on the machined surface on workpieces and saw teeth damages, which further enables the use of large positive rake angles for efficient cutting. The proposed mechanism will significantly advance current oscillating sawing techniques in bone cutting surgery and inspire tailored oscillating saw techniques for specific machining needs, such as thin deep groove cutting.

CRediT authorship contribution statement

Toshiyuki Enomoto: Writing – review & editing, Investigation. **Urara Satake:** Writing – review & editing, Investigation. **Han Wang:** Writing – original draft, Validation, Project administration, Methodology, Data curation, Conceptualization.

Declaration of Competing Interest

The authors declare the following financial interests/personal relationships which may be considered as potential competing interests: Han Wang, Urara Satake, Toshiyuki Enomoto has patent pending to Osaka University. If there are other authors, they declare that they have no known competing financial interests or personal relationships that could have appeared to influence the work reported in this paper

Acknowledgments

This study was partially supported by a Grant-in-Aid for Scientific Research (No. 24K00777, 2024) from the Ministry of Education, Culture, Sports, Science and Technology, Japan.

Appendix A. Supporting information

Supplementary data associated with this article can be found in the online version at doi:10.1016/j.jmatprotec.2024.118563.

References

[1] Axinte, D., Guo, Y., Liao, Z., Shih, A.J., M'Saoubi, R., Sugita, N., 2019. Machining of biocompatible materials - Recent advances. CIRP Ann. 68, 629–652. https://doi.org/10.1016/j.cirp.2019.05.003.

[2] James, T.P., Kelly, M.P., Lannin, T.B., Pearlman, J.J., Saigal, A., 2013. Sagittal bone saw with orbital blade motion for improved cutting efficiency. J. Med. Devices, Trans. ASME 7. https://doi.org/10.1115/1.4023500/376527.

[3] Plaskos, C., Hodgson, A.J., Inkpen, K., McGraw, R.W., 2002. Bone cutting errors in total knee arthroplasty. J. Arthroplast. 17, 698–705. https://doi.org/10.1054/arth.2002.33564.

[4] Kluess, D., Bergschmidt, P., Mueller, I., Mittelmeier, W., Bader, R., 2012. Influence of the distal femoral resection angle on the principal stresses in ceramic total knee components. Knee 19, 846–850. https://doi.org/10.1016/J.KNEE.2012.03.014.

[5] S.V. Vaidya, K.K. Dash, Tips and Pearls: Saw Technique in Total Knee Arthroplasty, in: Basics in Hip and Knee Arthroplasty, 2nd ed., 2017: pp. 222–229. https://shop.elsevier.com/books/basics-in-hip-and-knee-arthroplasty/vaidya/978-81-312-4888-1 (accessed April 24, 2024).

[6] O'donoghue, D.A., 2012. Surgical sagittal saw blade with spaced apart tines from which the blade teeth emerge and recessed webs that extend between the tines. United States patent.

[7] Shu, L., Sugita, N., 2020. Analysis of fracture, force, and temperature in orthogonal elliptical vibration-assisted bone cutting. J. Mech. Behav. Biomed. Mater. 103, 103599 https://doi.org/10.1016/J.JMBBM.2019.103599.

[8] Sugita, N., Mitsuishi, M., 2009. Specifications for machining the bovine cortical bone in relation to its microstructure. J. Biomech. 42, 2826–2829. https://doi.org/10.1016/J.JBIOMECH.2009.08.017.

[9] James, T.P., Chang, G., Micucci, S., Sagar, A., Smith, E.L., Cassidy, C., 2014. Effect of applied force and blade speed on histopathology of bone during resection by sagittal saw. Med. Eng. Phys. 36, 364–370. https://doi.org/10.1016/J.MEDENGPHY.2013.12.002.

[10] Tawy, G.F., Rowe, P.J., Riches, P.E., 2016. Thermal damage done to bone by burring and sawing with and without irrigation in knee arthroplasty. J. Arthroplast. 31, 1102–1108. https://doi.org/10.1016/j.arth.2015.11.002.

[11] Robles-Linares, J.A., Axinte, D., Liao, Z., Gameros, A., 2021. Machining-induced thermal damage in cortical bone: necrosis and micro-mechanical integrity. Mater. Des. 197, 109215 https://doi.org/10.1016/J.MATDES.2020.109215.

[12] Feczko, P.Z., Fokkenrood, H.J.P., van Assen, T., Deckers, P., Emans, P.J., Arts, J.J., 2017. Accuracy of the precision saw versus the sagittal saw during total knee arthroplasty: a randomised clinical trial. Knee 24, 1213–1220 https://doi.org/10.1016/j.knee.2017.07.018.

[13] Enomoto, T., Shigeta, H., Sugihara, T., Satake, U., 2014. A new surgical grinding wheel for suppressing grinding heat generation in bone resection. CIRP Ann. 63, 305–308. https://doi.org/10.1016/J.CIRP.2014.03.026.

[14] Gotterson, P.R., Nusem, I., Pearcy, M.J., Crawford, R.W., 2005. Metal debris from bony resection in knee arthroplasty - Is it an issue? Experiments in pigs. Acta Orthop. 76, 475–480. https://doi.org/10.1080/17453670510041448.
[15] M. Fisher, B. Chana, Surgical Saw Blade Device and System, 2014. https://patents.google.com/patent/US8672943B2/en (accessed December 22, 2022).
[16] Zhang, Y., Robles-Linares, J.A., Chen, L., Liao, Z., Shih, A.J., Wang, C., 2022. Advances in machining of hard tissues – From material removal mechanisms to tooling solutions. Int. J. Mach. Tools Manuf. 172, 103838 https://doi.org/10.1016/j.ijmachtools.2021.103838.
[17] Sugita, N., Osa, T., Aoki, R., Mitsuishi, M., 2009. A new cutting method for bone based on its crack propagation characteristics. CIRP Ann. 58, 113–118. https://doi.org/10.1016/J.CIRP.2009.03.057.
[18] Liao, Z., Axinte, D.A., 2016. On chip formation mechanism in orthogonal cutting of bone. Int. J. Mach. Tools Manuf. 102, 41–55. https://doi.org/10.1016/J.IJMACHTOOLS.2015.12.004.
[19] Feldmann, A., Ganser, P., Nolte, L., Zysset, P., 2017. Orthogonal cutting of cortical bone: temperature elevation and fracture toughness. Int. J. Mach. Tools Manuf. 118 (119), 1–11. https://doi.org/10.1016/J.IJMACHTOOLS.2017.03.009.
[20] Sugita, N., Ishii, K., Sui, J., Terashima, M., 2014. Multi-grooved cutting tool to reduce cutting force and temperature during bone machining. CIRP Ann. 63, 101–104. https://doi.org/10.1016/J.CIRP.2014.03.069.
[21] Liao, Z., Axinte, D.A., Gao, D., 2017. A novel cutting tool design to avoid surface damage in bone machining. Int. J. Mach. Tools Manuf. 116, 52–59. https://doi.org/10.1016/j.ijmachtools.2017.01.003.
[22] Shu, L., Li, S., Terashima, M., Bai, W., Hanami, T., Hasegawa, R., Sugita, N., 2020. A novel self-centring drill bit design for low-trauma bone drilling. Int. J. Mach. Tools Manuf. 154, 103568 https://doi.org/10.1016/J.IJMACHTOOLS.2020.103568.
[23] Sugita, N., Genma, F., Nakajima, Y., Mitsuishi, M., 2007. Adaptive Controlled Milling Robot for Orthopedic Surgery. in: Proceedings 2007 IEEE International Conference on Robotics and Automation. IEEE, pp. 605–610. https://doi.org/10.1109/ROBOT.2007.363053.
[24] Wang, H., Satake, U., Enomoto, T., 2022. Surgical oscillating saw blade to suppress forces in bone cutting. CIRP Ann. 71, 73–76. https://doi.org/10.1016/j.cirp.2022.04.066.
[25] Wang, H., Satake, U., Enomoto, T., 2023. Serrated chip formation mechanism in orthogonal cutting of cortical bone at small depths of cut. J. Mater. Process Technol. 319 https://doi.org/10.1016/j.jmatprotec.2023.118097.
[26] James, T.P., Pearlman, J.J., Saigal, A., 2012. Rounded cutting edge model for the prediction of bone sawing forces. J. Biomech. Eng. 134 https://doi.org/10.1115/1.4006972.
[27] Liao, Z., Axinte, D., Gao, D., 2019. On modelling of cutting force and temperature in bone milling. J. Mater. Process Technol. 266, 627–638. https://doi.org/10.1016/J.JMATPROTEC.2018.11.039.
[28] Song, X.F., Zhang, W., Kang, N., Zhao, J., Jing, X., 2023. Force prediction and analysis in surgical sawing of composite bone involving multi-tooth reciprocating and heterogeneous pore model. J. Mater. Process Technol. 312, 117853 https://doi.org/10.1016/J.JMATPROTEC.2022.117853.
[29] Wang, H., Satake, U., Enomoto, T., 2024. Modeling of oscillating bone sawing forces with instantaneous cutting speed and depth of cut. J. Mater. Process Technol. 324, 118225 https://doi.org/10.1016/J.JMATPROTEC.2023.118225.
[30] H.H. Fletcher, M.G. Fisher, Surgical Saw Blade, 2003. https://patents.google.com/patent/US6503253B1/en (accessed March 29, 2023).
[31] Hamilton, V., Sheikh, S., Szczepanska, A., Maskell, N., Hamilton, F., Reid, J.P., Bzdek, B.R., Murray, J.R.D., 2023. Diathermy and bone sawing are high aerosol yield procedures. Bone Jt. Res. 12, 636–643. https://doi.org/10.1302/2046-3758.1210.BJR-2023-0028.R1/LETTERTOEDITOR.
[32] S. Carusillo, Surgical Sagittal Saw Blade with Features That Facilitate Driving the Blade in A Crossed Loop Pattern, (2017). https://patents.google.com/patent/US9572585B2/en (accessed April 24, 2024).
[33] Shu, L., Sugita, N., Oshima, M., Mitsuishi, M., 2018. Design and experimental force analysis of a novel elliptical vibration assisted orthopedic oscillating saw. Med. Eng. Phys. 54, 22–31. https://doi.org/10.1016/j.medengphy.2018.02.005.
[34] Zhang, S., Chen, Z., Wu, H., Li, G., Wu, Y., 2023. Bone cutting processes and removal behaviors in orthopedic surgery with an ultrasonic orthopedic scalpel. Ultrasonics 131, 106966. https://doi.org/10.1016/J.ULTRAS.2023.106966.
[35] R.P. Winter, Knee Osteotomy Blade, 1975. https://patents.google.com/patent/US3905374A/en (accessed March 29, 2023).
[36] Son, S.M., Lim, H.S., Ahn, J.H., 2005. Effects of the friction coefficient on the minimum cutting thickness in micro cutting. Int. J. Mach. Tools Manuf. 45, 529–535. https://doi.org/10.1016/J.IJMACHTOOLS.2004.09.001.
[37] James, T.P., Pearlman, J.J., Saigal, A., 2013. Predictive force model for haptic feedback in bone sawing. Med. Eng. Phys. 35, 1638–1644. https://doi.org/10.1016/j.medengphy.2013.05.012.
[38] Choi, H.J., Yoon, H.K., Oh, H.C., Yoo, J.H., Choi, C.H., Lee, J.H., Park, S.H., 2021. Incidence and risk factors analysis for mortality after total knee arthroplasty based on a large national database in Korea. Sci. Rep. 11 (1 11), 1–9. https://doi.org/10.1038/s41598-021-95346-3.
[39] Foulke, B.A., Kendal, A.R., Murray, D.W., Pandit, H., 2016. Fracture healing in the elderly: a review. Maturitas 92, 49–55. https://doi.org/10.1016/j.maturitas.2016.07.014.
[40] Ngim, H.L.J., Van Bavel, D., De Steiger, R., Tang, A.W.W., 2023. Robotic-assisted revision total knee arthroplasty: a novel surgical technique. Arthroplasty 5. https://doi.org/10.1186/s42836-022-00160-5.
[41] Zhang, J., Cui, T., Ge, C., Sui, Y., Yang, H., 2016. Review of micro/nano machining by utilizing elliptical vibration cutting. Int. J. Mach. Tools Manuf. 106, 109–126. https://doi.org/10.1016/J.IJMACHTOOLS.2016.04.008.
[42] Shamoto, E., Suzuki, N., Hino, R., 2008. Analysis of 3D elliptical vibration cutting with thin shear plane model. CIRP Ann. 57, 57–60. https://doi.org/10.1016/J.CIRP.2008.03.073.
[43] Shamoto, E., Moriwaki, T., 1994. Study on elliptical vibration cutting. CIRP Ann. 43, 35–38. https://doi.org/10.1016/S0007-8506(07)62158-1.
[44] Robles-Linares, J.A., Liao, Z., Axinte, D., Gameros, A., 2022. The effect of interstitial fluid on the machining behaviour of cortical bone. J. Mater. Process Technol. 307, 117697 https://doi.org/10.1016/J.JMATPROTEC.2022.117697.
[45] Anderson, D., Warkentin, A., Bauer, R., 2011. Experimental and numerical investigations of single abrasive-grain cutting. Int. J. Mach. Tools Manuf. 51, 898–910. https://doi.org/10.1016/J.IJMACHTOOLS.2011.08.006.
[46] Danova, N.A., Colopy, S.A., Radtke, C.L., Kalscheur, V.L., Markel, M.D., Vanderby, R., McCabe, R.P., Escarcega, A.J., Muir, P., 2003. Degradation of bone structural properties by accumulation and coalescence of microcracks. Bone 33, 197–205. https://doi.org/10.1016/S8756-3282(03)00155-8.
[47] Zimmermann, E.A., Gludovatz, B., Schaible, E., Busse, B., Ritchie, R.O., 2014. Fracture resistance of human cortical bone across multiple length-scales at physiological strain rates. Biomaterials 35, 5472–5481. https://doi.org/10.1016/J.BIOMATERIALS.2014.03.066.
[48] Chen, Q., Li, D.Y., 2005. A computational study of frictional heating and energy conversion during sliding processes. Wear 259, 1382–1391. https://doi.org/10.1016/J.WEAR.2004.12.025.
[49] Bai, X., Hou, S., Li, K., Qu, Y., Zhu, W., 2020. Analysis of machining process and thermal conditions during vibration-assisted cortical bone drilling based on generated bone chip morphologies. Med. Eng. Phys. 83, 73–81. https://doi.org/10.1016/j.medengphy.2020.07.016.
[50] Bai, W., Shu, L., Sun, R., Xu, J., Silberschmidt, V.V., Sugita, N., 2020. Mechanism of material removal in orthogonal cutting of cortical bone. J. Mech. Behav. Biomed. Mater. 104, 103618 https://doi.org/10.1016/j.jmbbm.2020.103618.
[51] Gao, P., Zhao, X., Wang, M., Gao, X., Zan, T., Jing, L., 2024. Crack propagation determined by energy release rate in cortical bone ultrasonic vibration assisted cutting. J. Mater. Process Technol. 330, 118453 https://doi.org/10.1016/J.JMATPROTEC.2024.118453.
[52] Maradia, U., Kliuev, M., Baumgart, C., 2018. Efficient machining of complex-shaped seal slots for turbomachinery. CIRP Ann. 67, 209–212. https://doi.org/10.1016/J.CIRP.2018.04.099.